

https://dspace.org/

The MerenskyBastard interval at Hackney eastern Bushveld Complex results of a combined SrNdisotopic investigation

J Magson; F Roelofse; Grant Bybee; Robert Bolhar

SPRINGER
https://hdl.handle.net/10539/40923
WOS

Downloaded from a DSpace repository. https://dspace.org/

Contributions to Mineralogy and Petrology (2024) 179:72
https://doi.org/10.1007/s00410-024-02155-8

ORIGINAL PAPER

The Merensky-Bastard interval at Hackney, eastern Bushveld Complex: results of a combined Sr–Nd-isotopic investigation

Justine Magson[1] · **Frederick Roelofse**[1] · **Grant Bybee**[2] · **Robert Bolhar**[2]

Received: 3 April 2024 / Accepted: 14 June 2024
© The Author(s) 2024

Abstract

The Merensky and Bastard reefs of the Bushveld Complex occur within what has been called a transitional macro-unit along the boundary of the Critical and Main zones. The transitional unit is characterised by a geochemical hiatus recording distinct inflections in mineral chemistry and isotopic compositions. Previously these inflections in mineral chemistry and changes in isotopic compositions were attributed mostly to the influx of a magma that was compositionally distinct from the resident magma and that was parental to the Main Zone of the complex. Sr-isotopic variations across this interval have been particularly well-studied, but despite this, little consensus exists regarding the petrogenesis and metallogenesis of this economically important interval. Here we report whole-rock Sr–Nd-isotopic, major- and trace element geochemical and mineral chemical data across the Merensky-Bastard interval as intersected by borehole BH8172 on the farm Hackney in the eastern Bushveld Complex. Variations in whole-rock Cr/MgO values and initial Sr isotopic ratios across the interval are consistent with the results of previous studies that argued for the co-accumulation of minerals from compositionally and isotopically distinct magmas, of Critical and Main Zone lineages, respectively. In our model, a magma of Critical Zone affinity enters the chamber causing erosion along the chamber floor. Orthopyroxene and plagioclase crystallise from the Critical Zone magma to form the Merensky Reef, as suggested by high whole-rock Cr/MgO ratios (> 80) and unradiogenic Sr-isotopic compositions ($^{87}Sr/^{86}Sr_i < 0.7068$). A plagioclase-laden magma of Main Zone affinity subsequently intruded the chamber as a basal flow, elevating the resident Critical Zone magma. Plagioclase within the former floated, forming a solid raft onto which the Bastard Reef was deposited, a model that is entirely consistent with density considerations and an upward increase in the An-content of plagioclase as observed in the anorthositic package between the Merensky and Bastard reefs. From a metallogenetic viewpoint, this would imply that the Main Zone could not have been the source of the PGEs within the Merensky Reef.

Keywords Bastard Reef · Eastern Bushveld Complex · Merensky Reef · Sm–Nd · Rb–Sr

Introduction

The Merensky Reef of the Bushveld Complex has been extensively studied since its discovery in 1924 (Cawthorn 1999). Despite a century of investigation, little consensus exists regarding its petrogenesis and metallogenesis (Latypov et al. 2015; Smith et al. 2021). The reef represents the largest platinum reserve in the world (Cawthorn 1999, 2010; Viljoen 2016), especially when taking into account the recently discovered Flatreef deposit of the Northern Limb of the Bushveld Complex, which recent work (Grobler et al. 2019; Beukes et al. 2021; Keet et al. 2021, 2024; Mayer et al. 2021) has shown to be an equivalent of the Merensky Reef in the better studied Eastern and Western limbs of the complex.

The chromite- and sulphide-bearing, mostly orthopyroxenitic Merensky Reef exhibits considerable lateral variation in terms of the thickness of the reef, where within the reef mineralisation is located and in terms of the lithologies encountered within the foot- and hangingwalls and within the reef itself, the latter complicated by the reef locally cutting meters to several tens of meters into footwall rocks that

Communicated by Dante Canil.

✉ Justine Magson
markramj1@ufs.ac.za

[1] Department of Geology, University of the Free State, P.O. Box 339, Bloemfontein 9300, South Africa

[2] School of Geosciences, University of the Witwatersrand, Private Bag 3, WITS, Johannesburg 2050, South Africa

Published online: 24 June 2024

may result in circular depressions known as potholes (Cawthorn and Boerst 2006; Latypov et al. 2015). Despite the complicated nature of the reef, the Merensky and overlying lithologically similar but unmineralized (and therefore aptly named) Bastard reefs can be traced for distances of over 100 km in both the Eastern and Western limbs and are potentially continuous at depth from east to west (Hunter 1987; Cawthorn and Boerst 2006; Hunt et al. 2018).

Platinum Group Element (PGE) mineralisation within the Merensky Reef appears to be the culmination of an upward trend of chromitite-hosted Pt + Pd enrichment throughout the Critical Zone of the Bushveld Complex (Scoon and Teigler 1994; Maier et al. 2013), an observation that argues strongly against models invoking emplacement of the Merensky Reef and other rock layers as out-of-sequence sills (*cf.* Mitchell and Scoon 2007; Mungall et al. 2016; Latypov et al. 2018; Scoates et al. 2021). Some debate surrounds the position at which the Merensky Reef should be placed stratigraphically within the Bushveld Complex, with most authors placing it and the Bastard Reef within the upper reaches of the Upper Critical Zone (e.g. Eales and Cawthorn 1996; Naldrett et al. 2009; Smith et al. 2021). Dissenting views include those of Kruger (1990), who proposed that the "Merensky Cyclic Unit", a concept that has since been challenged (Hunt et al. 2018), should be taken as the basal unit of the Main Zone.

The Merensky and Bastard reefs occur within what has been called a transitional macro-unit along the boundary of the Critical and Main zones (e.g. Kruger 1992). The transitional unit is characterised by distinct inflections in mineral chemistry and isotopic compositions that most authors attribute to the influx of a magma that was compositionally distinct from the resident magma and that was parental to the Main Zone of the complex. Authors have attributed the resident magma at this level of the intrusion to the B2 magma or potentially to a mixture between B1 and B2 magmas, whereas the magma parental to the Main Zone has mostly been attributed to the B3 magma as inferred from the suite of marginal rocks (Barnes et al. 2010). Sr-isotopic variations across this transitional interval have been particularly well-studied at numerous sites on both the Eastern (Lee and Butcher 1990; Seabrook et al. 2005) and Western (Kruger and Marsh 1982; Eales et al. 1986, 1990; Kruger 1992; Yang et al. 2013; Karykowski et al. 2017; Smith et al. 2021) limbs, with the interval recording an upward change in initial $^{87}Sr/^{86}Sr$ ratios from Upper Critical Zone values on the order of 0.7060–0.7068 in the footwall of the Merensky Reef to Lower Main Zone values in excess of 0.7075 (Seabrook et al. 2005). The interval also records changes in the Sr content of plagioclase from Upper Critical Zone values of > 450 ppm to Lower Main Zone values of < 400 ppm, and in the Cr content of orthopyroxene from Upper Critical Zone values of > 2500 ppm to Lower Main Zone values of ~ 1000 ppm (Seabrook et al. 2005).

Both inter- and intracrystalline mineral disequilibrium across the transitional interval hosting the Merensky and Bastard reefs has been reported (Prevec et al. 2005; Seabrook et al. 2005; Yang et al. 2013). The existence of mineral disequilibrium suggests that the interval did not form through simple mixing of melts, but rather in response to the incorporation of minerals crystallised from different melts into the rocks constituting this interval. The present study is aimed at augmenting the rather limited combined Sr- and Nd-isotopic dataset for the Bushveld Complex across the Merensky and Bastard reefs at Hackney on the Central Sector of the Eastern Limb, with a view on improving our understanding of the petrogenetic processes involved in the formation of this economically important transitional interval.

Overview of existing models for the petrogenesis and metallogenesis of the Merensky Reef

Latypov et al. (2015) provided a summary of models that have been proposed to account for the formation of the Merensky Reef and its PGE enrichment. Turbulent mixing models (Campbell et al. 1983; Naldrett 1989) suggest that the Merensky Reef formed in response to large-scale turbulent mixing of resident and newly added magma and the subsequent settling of droplets of immiscible sulphide melt and chromite crystals onto the temporary floor of the magma chamber. Lateral mixing models (Scoon and Teigler 1994; Naldrett et al. 2011) invoke the emplacement of magma as basal flows onto the temporary chamber floor. Kinnaird et al. (2002) proposed that the chamber was contaminated by granophyric roof rock melts that were entrained by a batch of magma that entered the chamber in the form of a fountain, leading to the crystallisation of both chromite and PGMs subsequently carried onto the floor of the chamber along the descending margins of the magma fountain. Cawthorn (2005, 2011) argued that magma mixing was not a prerequisite for saturating the magma in sulphur and chromite, proposing instead that both could be achieved in response to a transient increase in pressure throughout the chamber due to the introduction of a basal influx of magma. Latypov et al. (2015) suggested that the Merensky Reef formed in response to repeated basal inflows of magma that thermochemically eroded the cumulate pile and that crystallised in-situ on the chamber floor. They further suggested that in-situ grown chromite and sulphide melt scavenged PGEs from the overlying magma during vigorous thermochemical convection.

All the aforementioned models have in common the introduction of a new magma (or new magmas) into the chamber at a level above the immediate chamber floor, essentially leading to sulphur saturation either in response to mixing or

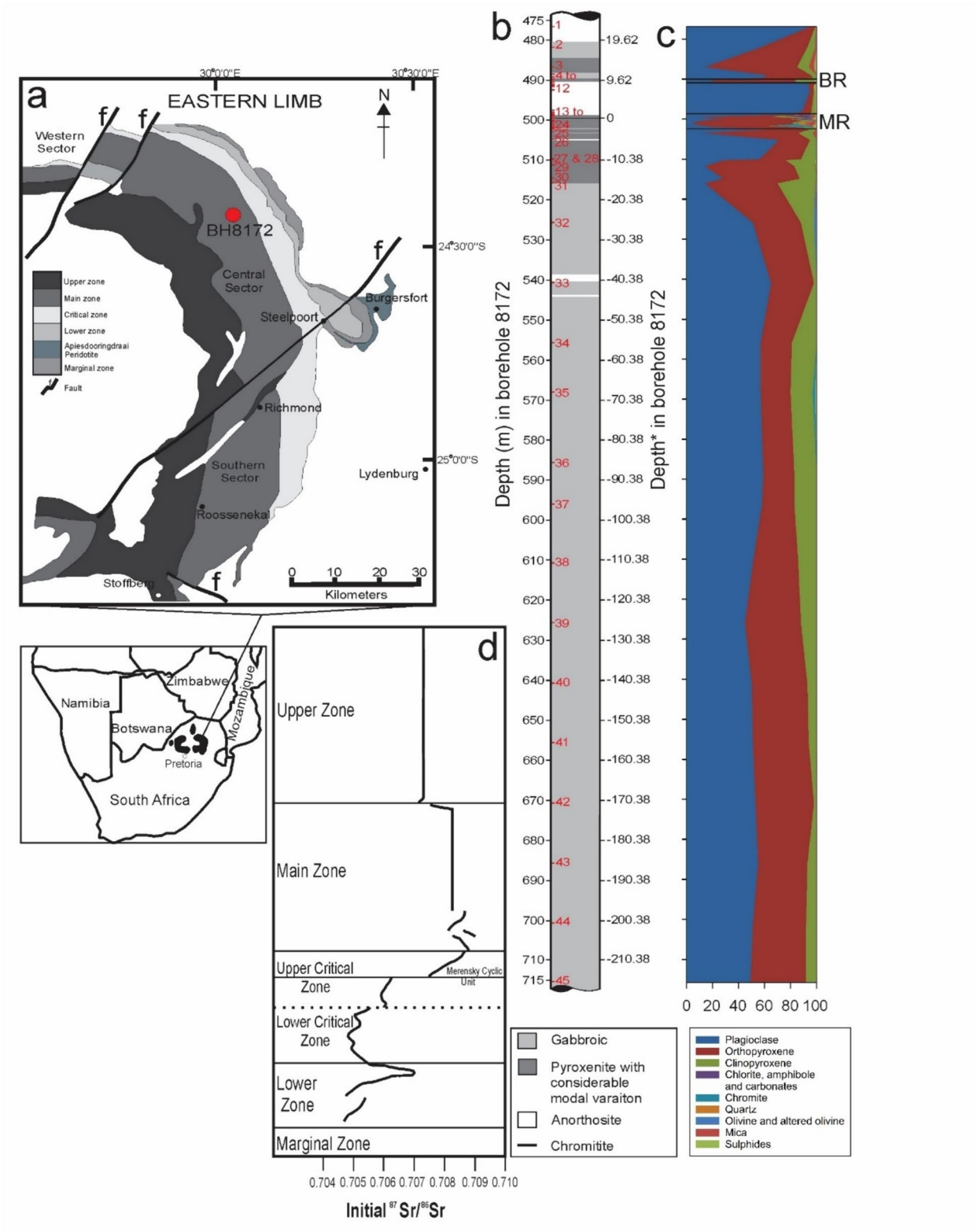


Fig. 1 **a** Map showing the extent of the Rustenburg Layered Suite (RLS) in South Africa and the geology of the Eastern Limb of the RLS along with the position of borehole BH8172. Map is modified after Cameron & Abendroth (1957). **b** & **c** Logs showing the variation in lithology and mineral modes across the studied interval along with the locations where samples were taken. *Numbers refer to depth in meters in borehole relative to the base of the top Merensky chromitite stringer. **d** Sr-isotopic variations through the RLS on the Western Limb of the Bushveld Complex as per Kruger (1994)

increased pressure in the chamber. Implicit in these models is the notion that the magma overlying the Merensky Reef (and from which the Main Zone presumably crystallised) was the source of the PGEs concentrated in the Merensky Reef and that the Main Zone should therefore be depleted in PGEs. These models all belong to the "downers" school of thought, which suggests that PGEs were concentrated on the immediate floor of the chamber, having been scavenged from the overlying magma column (Naldrett et al. 2009).

The "uppers" school of thought maintains that PGE enrichment in the Merensky Reef happened in response to the remobilisation of PGEs and sulphur from the underlying cumulate pile through the action of volatile-rich fluids (Naldrett et al. 2009). Sulphur saturation was achieved when the fluid mixed with the resident magma overlying the cumulate pile, with the resident magma acting as a source of additional PGEs. Proponents of this school of thought include Willmore et al. (2000), Boudreau & McCallum (1992) and Mathez et al. (1997), amongst others.

A third and relatively recent school of thought, termed "off-stage" developed over the course of the last decade. This school of thought maintains that the concentration of the PGEs present within the Merensky Reef occurred outside of the known Bushveld magma chamber, within a sub-Bushveld staging chamber(s) that has been postulated to exist on the basis of geochemical evidence (e.g. Ashwal et al. 2005; Eales and Costin 2012; Maier et al. 2013; McDonald and Holwell 2007; Prevec et al. 2005; Roelofse and Ashwal 2012; Wilson 2012; Roelofse et al. 2015; Beukes et al. 2021; Keet et al. 2021, 2024; Yao et al. 2021), augmented by recent geophysical interpretations (Cole et al. 2024). Proponents of this school of thought include Hutchinson et al. (2015) and Magson et al. (2023).

The models of Mitchell & Scoon (2007), Kruger (2010), Maier et al. (2013) and Mungall et al. (2016) cannot be clearly assigned to any of the three schools of thought mentioned. Mitchell and Scoon (2007), Kruger (2010) and Mungall et al. (2016) postulated that the Merensky Reef was intruded as a sill into the existing cumulate pile. Kruger (2010) proposed that the magma was of a Main Zone lineage and that it intruded beneath an already existing Bastard Reef. Mitchell and Scoon (2007) suggested that the Merensky Reef, and most of the thick, laterally persistent chromitite layers of the Critical Zone, were sequentially emplaced as sills into the developing cumulate pile, with both the sills and the intervening layers recording evidence for simultaneous but distinct compositional evolution with time. Mungall et al. (2016), relying on precise U–Pb zircon dating, suggested that the Merensky Reef postdates the Main Zone of the complex and thus had to be intruded as a sill into pre-existing mafic rocks. Out-of-sequence ages were also reported by Scoates et al. (2021). The results, however, appear to be ambiguous when taking into account field relationships (Latypov et al. 2017; Mitchell 2021) and have therefore not seen widespread acceptance.

Maier et al. (2013) proposed a fundamentally different mechanism for the origin of stratiform reef horizons (including chromitite and magnetitite layers) within the Bushveld Complex, arguing that they formed in response to the hydrodynamic concentration of sulphides, chromite and magnetite during the collapse of cumulate layers due to crustal loading and central subsidence of the magma chamber.

Geology and samples from the Hackney drill site

Borehole BH8172 was drilled on the farm Hackney, by Impala Platinum in 2012. It is a 915 m deep hole drilled on the Central Sector of the Eastern Limb (Fig. 1). It is collared in the Lower Main Zone and extends below the footwall of the Merensky Reef in the Upper Critical Zone. The core is currently curated by the Department of Geology at the University of the Free State as part of the BVDP drilling project funded by the International Continental Scientific Drilling Program (ICDP) (Trumbull et al. 2015). A total of 45 samples were collected from the core, covering the depth interval between 476.56 m and 715.33 m in borehole BH8172 as part of this study. In this contribution we define the Merensky Reef as the pyroxenite bounded by two chromitite stringers along with an underlying pegmatoidal melagabbronorite layer (to about – 2.48 m) and an overlying pegmatoidal pyroxenite (to about + 0.75 m), the latter transitioning into an anorthosite that forms the hangingwall of the Merensky Reef and the footwall of the Bastard Reef (Electronic Appendix A.1). The uppermost Merensky chromitite stringer is represented by a 1 mm thin chromitite stringer with a sharp lower contact, occurring at a depth of 499.62 m. The base of the uppermost Merensky chromitite stringer was used as the reference datum for the profiles presented in this study. The lower, irregular chromitite stringer (at – 1.69 m) consists of disseminated chromite with a thickness of up to ~ 15 mm. The Merensky Reef is overlain by the leuconoritic to anorthositic Merensky Reef hangingwall / Bastard Reef footwall, which is spotted towards its base, becoming mottled higher up. The base of the Bastard Reef is marked by a thin chromitite stringer at 490.48 m (+ 9.14 m), that is overlain by pyroxenite that grades upwards into melagabbronorite extending to about + 9.94 m, that we define as the upper extent of the Bastard Reef. The upper contact of the Bastard Reef is not well-defined. There is a general tendency for the rocks overlying the Bastard Reef to become more felsic with height, with (gabbro)noritic rocks being replaced first by spotted anorthosite and then mottled anorthosite in a sequence of rocks that looks remarkably similar to the sequence that occurs between the Merensky and Bastard reefs.

Methods

Petrography

Forty-five polished thin sections were prepared and subjected to optical petrographic examination using transmitted and reflected light microscopy. High-resolution scans were taken at the University of the Witwatersrand with the Olympus BX53M/DP74 microscope. A digitized point grid was placed over each scan and used for point counting (counting 300 points). Minerals that were encountered under the microscope but not in point counting were assigned concentrations of less than 0.5% by volume.

Mineral chemistry

Forty-five samples were used for quantitative mineral chemical analyses of feldspar and pyroxene using four wavelength dispersive spectrometers on a JEOL JXA-8230 electron probe micro-analyser at Rhodes University. A detailed description of experimental procedures was reported in Magson et al. (2023). Between three and four analyses of plagioclase, orthopyroxene and clinopyroxene were performed on each sample, with one analysis spot per crystal centred on the apparent core of each crystal.

Whole-rock trace element geochemistry

A Thermo Scientific iCAP RQ Inductively Coupled Plasma Mass Spectrometer (ICP-MS) housed in the Earth Observatory of the University of the Witwatersrand was used for trace element analysis following the procedures detailed in Magson et al. (2023). Total procedural blanks (TPBs) and Certified Reference Materials (BCR-1, BHVO-2 and BIR-1) were analysed along with all unknowns for quality control (see Electronic Appendix B.1).

Whole-rock major element geochemistry

X-ray Fluorescence Spectrometry was used for the determination of the whole-rock major element geochemistry of samples as per the method described in Magson et al. (2023). Certified Reference Materials (NIM-N (SARM 4) and NIM-P (SARM 5)) were used to monitor the accuracy and precision of the analyses. Repeatability for the major elements obtained on replicates and expressed as percentage relative standard deviations (%RSDs) were all less than ~ 4% for SARM 5 and less than 5% for SARM 4 (except for P_2O_5, 9.07%). Relative errors for all oxides compared to the accepted values for the SARM 5 standard were all below 3%, except for Na_2O (+ 9.5%), K_2O (– 8.9%) and P_2O_5 (– 6%). For SARM 4, relative errors were all below 4%, except for Na_2O (– 10.6%) and P_2O_5 (– 10%) (see Electronic Appendix B.2).

Isotopic determinations

A total of 21 samples were chosen for whole-rock Rb–Sr and Sm–Nd isotopic determinations. Approximately 100 – 350 mg of sample was weighed off and different volumes of ^{85}Rb-^{84}Sr and ^{149}Sm-^{150}Nd spikes were added and then dissolved in a mixture of HF-HNO_3. Sr and Rb separation took place in 2 ml BioRad AG50 × 8, 200–400 mesh resin columns. Sm and Nd were separated in 1 ml Eichrom Ln Spec 100–150 µm resin columns. The Sm–Nd isotopic compositions of samples were measured in low resolution mode on a Nu Instruments Plasma II MC-ICP-MS, housed at the Spectrum analytical facility (University of Johannesburg). Backgrounds were measured and subtracted from the measurements. Sm measurements were collected for 20 cycles and Nd for 60 cycles, giving an internal precision of $< \pm 0.002\%$ (1 standard error). Total procedural blanks and two Certified Reference Materials (BCR-2 and BHVO-2) were included in the analyses to ensure quality and reproducibility (see Electronic Appendix B.3 & B.4).

Strontium isotopic compositions were measured on a Nu Instruments Thermal Ionisation Mass Spectrometer housed in the Earth Observatory in School of Geosciences, University of the Witwatersrand. The instrument is equipped with 16 fixed Faraday detectors and a zoom lens system allowing for the alignment of isotopes into adjacent collectors. Strontium was loaded onto outgassed zone-refined Re filaments in ~ 1 µl 0.5N HNO_3 and ~ 1 µl TaF_5 activator between two Parafilm strips. The sample filament was heated slowly to 2400–3000 mA to obtain stable Sr signals. Strontium isotope ratios were collected in a 3-line dynamic measurement, with time drift correction, following methods similar to Luu et al. (2022). During Sr isotope analyses, Faraday detectors were connected to amplifiers with 10^{11} Ω resistors. In the first line, ^{88}Sr was collected in H9, followed by H7 in line 2, and H5 in line 3. The ^{85}Rb signal was used to correct for the isobaric interference of ^{87}Rb on ^{87}Sr using the normal $^{87}Rb/^{85}Rb$ ratio of 0.3857. Instrumental mass fractionation was corrected using $^{86}Sr/^{88}Sr$ of 0.1194. Repeated analyses of the SRM987 standard yielded a value of 0.710251 ± 0.000068 (95 ppm; 2SD of 29 measurements between Aug '22 and Feb '23), with an accepted value of 0.710247 ± 0.000004 (Luu et al. 2022). Standard error (SE) uncertainties are reported as the in-run precision. Blank contributions to the signal were negligible.

Rubidium isotopic compositions were measured on a Nu Instruments Sapphire multi-collector ICP-MS in the School of Geosciences, University of the Witwatersrand. The instrument is equipped with 16 fixed Faraday detectors and a zoom

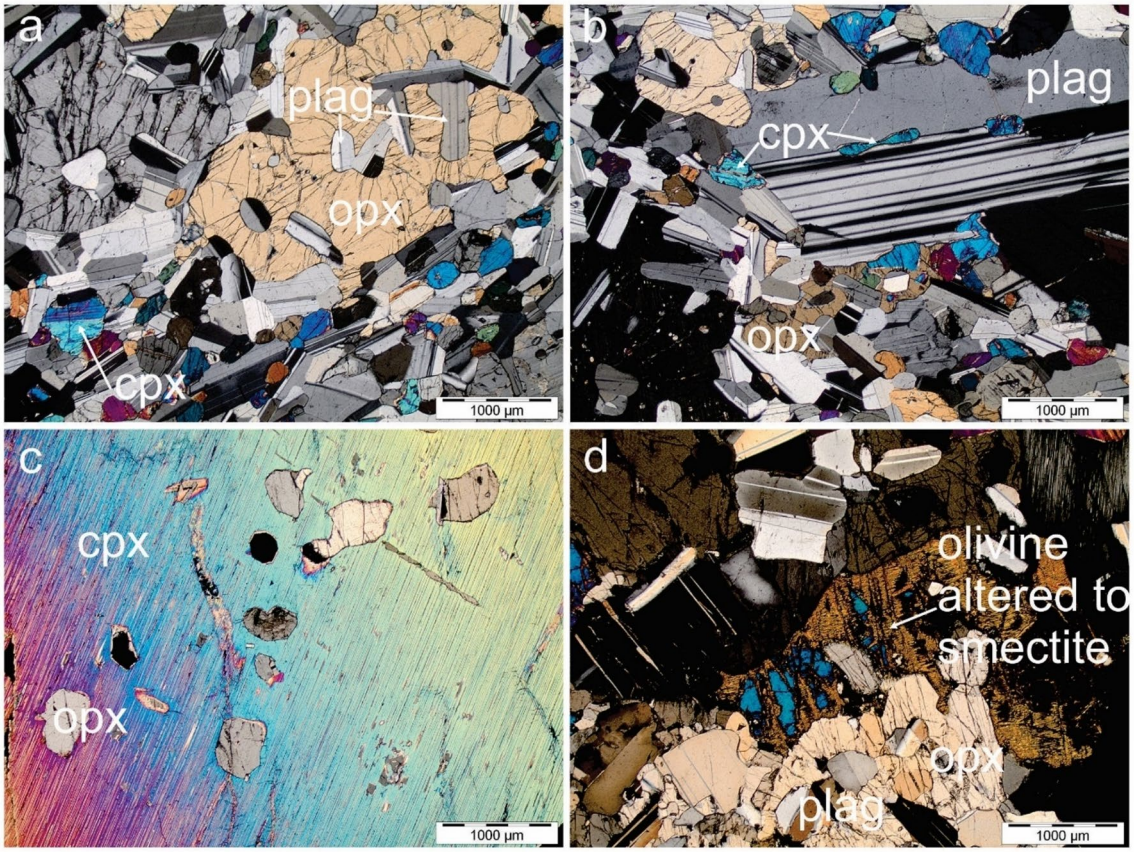


Fig. 2 **a** Photomicrograph of gabbronorite from depth – 96.43 m showing ophitic texture as defined by plagioclase chadacrysts occurring enclosed within orthopyroxene oikocrysts. **b** Photomicrograph of gabbronorite from depth – 111.09 m showing inclusions of clinopyroxene in plagioclase crystal with wedge-shaped deformation twins. **c** Photomicrograph of melagabbronorite from depth – 11.78 m showing a large (>6 mm) clinopyroxene oikocryst enclosing orthopyroxene chadacrysts. **d** Photomicrograph of gabbronorite from depth – 25.96 m showing olivine altered to smectite and orthopyroxene enclosing plagioclase. All images taken under cross polarized, transmitted light. (*opx* orthopyroxene; *cpx* clinopyroxene; *plag* plagioclase)

lens system allowing for the alignment of isotopes into adjacent collectors. Rubidium was taken up into 5 ml 2% HNO_3 and analysed using an Apex desolvating nebuliser with the following conditions: coolant Ar flow 18 l/min, auxiliary Ar flow 0.9–1.2 l/min, nebuliser Ar flow 1.15–1.2 l/min, apex Ar flow 3.81–3.89 l/min. Rubidium isotope ratios were collected during a static measurement of 50 cycles, with ^{87}Rb on L1 and ^{85}Rb on L5. Mass 88 was monitored on H1 in order to correct for any ^{87}Sr interferences on ^{87}Rb, using an $^{87}Sr/^{88}Sr$ ratio of 0.08478. Mass fractionation was corrected with sample-standard bracketing of a natural Rb solution, using the normal $^{87}Rb/^{85}Rb$ of 0.38571. Standard error (SE) uncertainties are reported as the in-run precision. Blank contributions to the signal were negligible.

Initial $^{87}Sr/^{86}Sr$ and $^{143}Nd/^{144}Nd$ ratios were calculated using decay constants of 1.42×10^{-11} y^{-1} (Steiger and Jäger 1977) and 6.54×10^{-12} y^{-1} (Begemann et al. 2001), respectively, for an age of 2.055 Ga (Zeh et al. 2015). ε_{Ndi} values were calculated using values for CHUR of $^{143}Nd/^{144}Nd = 0.512638$ (Goldstein et al. 1984) and $^{147}Sm/^{144}Nd = 0.1967$ (Jacobsen and Wasserburg 1980). No significant variations in ε_{Ndi} values are apparent when using the more recent CHUR values of Bouvier et al. (2008).

Results

Petrography

Electronic Appendix B.5 contains a summary of the mineral modes, grain sizes and additional petrographic observations. Twenty-two samples were collected from the sequence of rocks underlying the Merensky Reef, with most being gabbroic to noritic in composition. Fourteen gabbronorites; 5 melagabbronorites, 1 leucogabbronorite, 1 leuconorite and 1 norite were encountered. The more felsic gabbroic to noritic rocks generally have a spotted appearance due to the presence of subhedral to anhedral crystals of pyroxene.

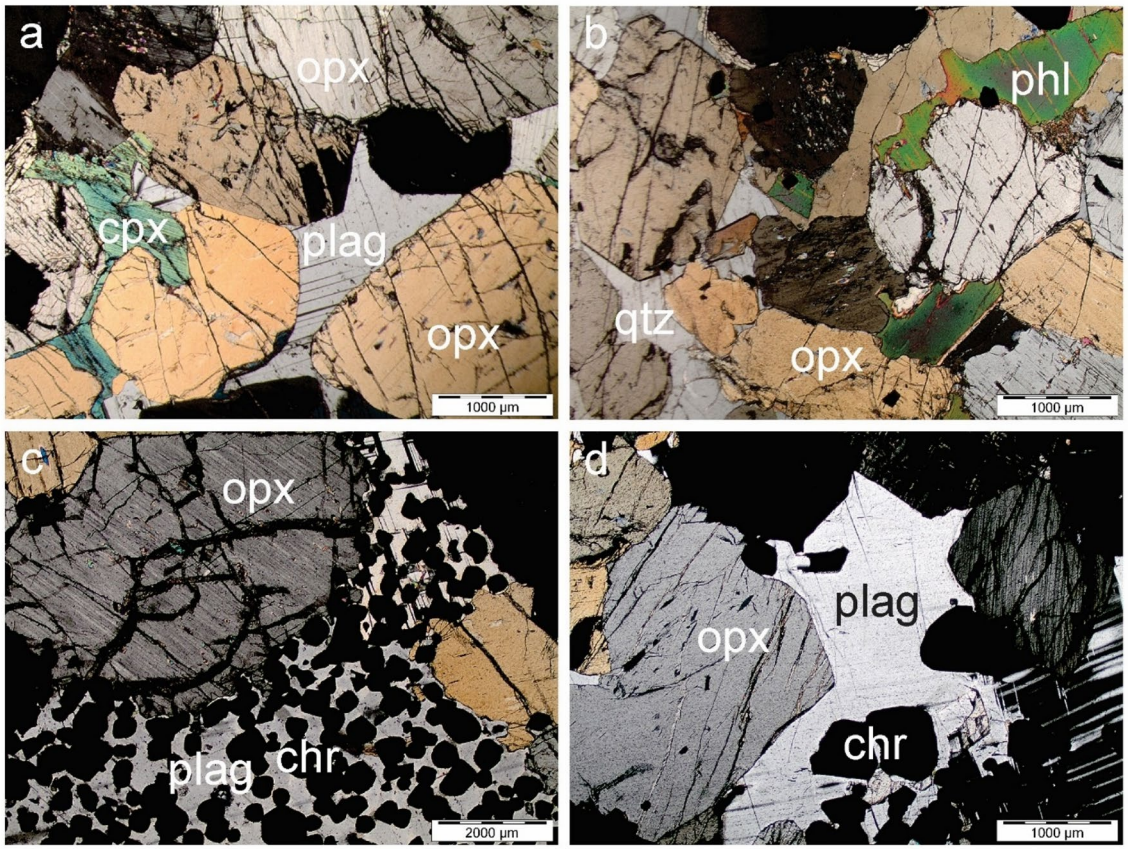


Fig. 3 **a** Photomicrograph of melanorite from depth – 1.69 m showing the apparently intercumulus nature of plagioclase within the Merensky Reef. **b** Photomicrograph of pyroxenite from depth – 1.3 m showing the presence of phlogopite and interstitial quartz. **c** Photomicrograph of the lower Merensky chromitite stringer from depth – 1.69 m showing the close association between chromite and intercumulus plagioclase. **d** Photomicrograph of the upper Merensky chromitite stringer hosting chromite that tends to be coarser grained than that encountered in the lower chromitite stringer. All images were taken under cross polarized, transmitted light. (*opx* orthopyroxene; *cpx* clinopyroxene; *plag* plagioclase; *chr* chromite; *qtz* quartz; *phl* phlogopite)

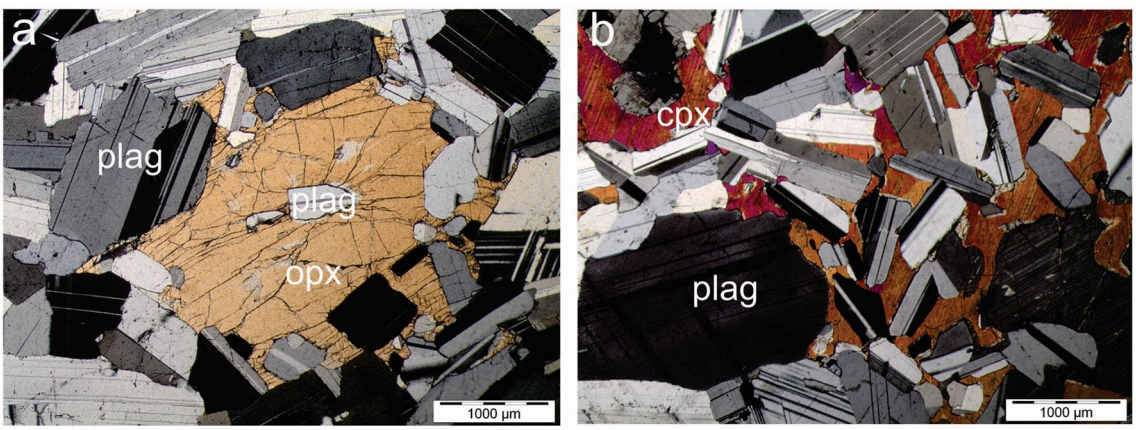


Fig. 4 **a** Photomicrograph of anorthosite from depth + 1.87 m showing an orthopyroxene oikocryst enclosing plagioclase chadacrysts. **b** Photomicrograph of leuconorite from depth + 1.08 m showing a large clinopyroxene oikocryst enclosing plagioclase chadacrysts. Both images taken under cross polarized, transmitted light. (*opx* orthopyroxene; *cpx* clinopyroxene; *plag* plagioclase)

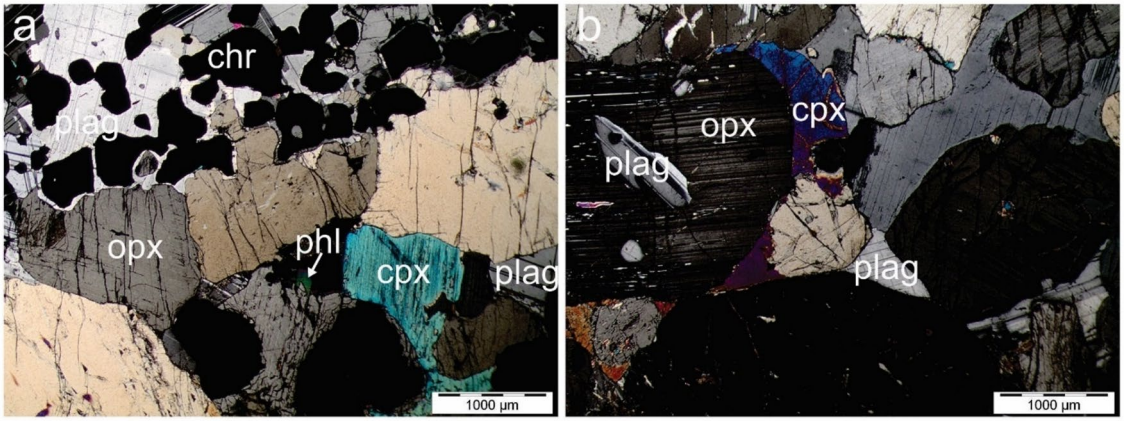


Fig. 5 **a** Photomicrograph showing thin chromitite stringer straddling the contact between the Bastard pyroxenite (lower right) at depth + 9.14 m and the underlying anorthosite (upper left). **b** Photomicrograph of melagabbronorite from depth + 9.94 m showing intercumulus plagioclase occurring interspersed with orthopyroxene and as inclusions within orthopyroxene. Both images were taken under cross polarized, transmitted light. (*opx* orthopyroxene; *cpx* clinopyroxene; *plag* plagioclase; *chr* chromite; *phl* phlogopite)

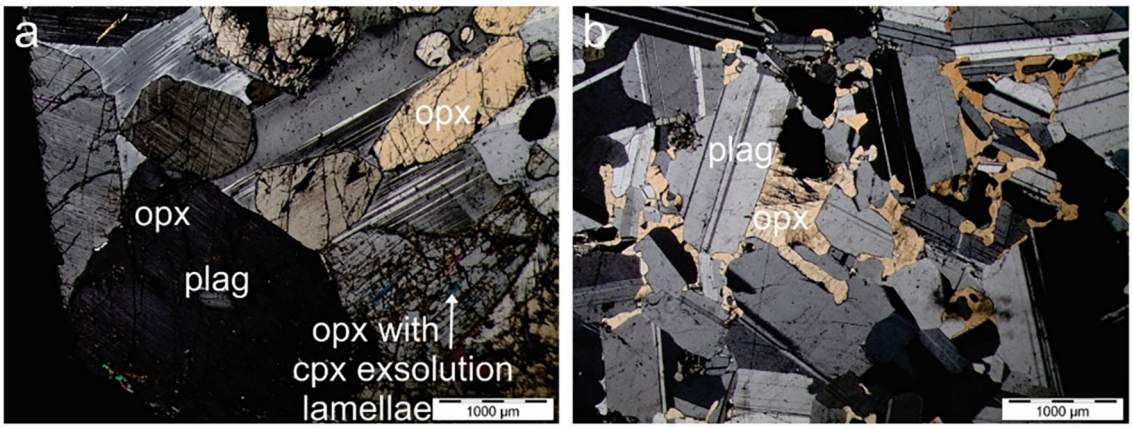


Fig. 6 **a** Photomicrograph of melagabbronorite from depth + 12.97 m showing orthopyroxene crystals containing thin and narrowly spaced exsolution lamellae of clinopyroxene, occurring enclosed within an optically continuous plagioclase crystal **b** Photomicrograph of anorthosite from depth + 23.06 m showing plagioclase enclosed within an orthopyroxene oikocryst. This textural arrangement would manifest as mottling when viewed macroscopically. Both images were taken under cross polarized, transmitted light. (*opx* orthopyroxene; *cpx* clinopyroxene; *plag* plagioclase)

Orthopyroxene modally constitutes 23 – 74% of the samples, with maximum grain sizes varying between ~ 1 and 3 mm. Ophitic to sub-ophitic textures are commonly encountered (Fig. 2a). Orthopyroxene normally contains narrowly spaced exsolution lamellae of clinopyroxene. Plagioclase modally constitutes 12–71% of individual samples and occurs as abundantly twinned laths. Maximum plagioclase grain sizes vary from ~ 1 to 1.5 mm. Inclusions of clinopyroxene in plagioclase are commonly encountered (Fig. 2b). Zonation in plagioclase was not observed optically. Plagioclase chadacrysts in the orthopyroxene are small and randomly orientated, compared to the coarser laminated laths, not included in orthopyroxene. Anhedral clinopyroxene modally constitutes between 2 and 29% of the samples studied. Clinopyroxene typically contains thick orthopyroxene exsolution lamellae (Fig. 2c) and is twinned in many cases (Fig. 2a). Maximum grain sizes vary from < 1 mm to > 6 mm. Olivine and olivine altered to smectite was observed in a single gabbronorite sample from depth – 25.96 m (Fig. 2d). Minor phlogopite, chromite and sulphides were observed in some samples.

Nine samples were collected from the Merensky Reef (as defined herein) and shown to consist of 1 pegmatoidal melagabbronorite (constituting the lowermost sample collected), 3 melanorites, 2 pyroxenites, 1 altered pegmatoidal pyroxenite, 1 altered melagabbronorite and 1 melagabbronorite. Plagioclase modally constitutes between 5 and 34% of the samples and appears to be intercumulus in the majority of

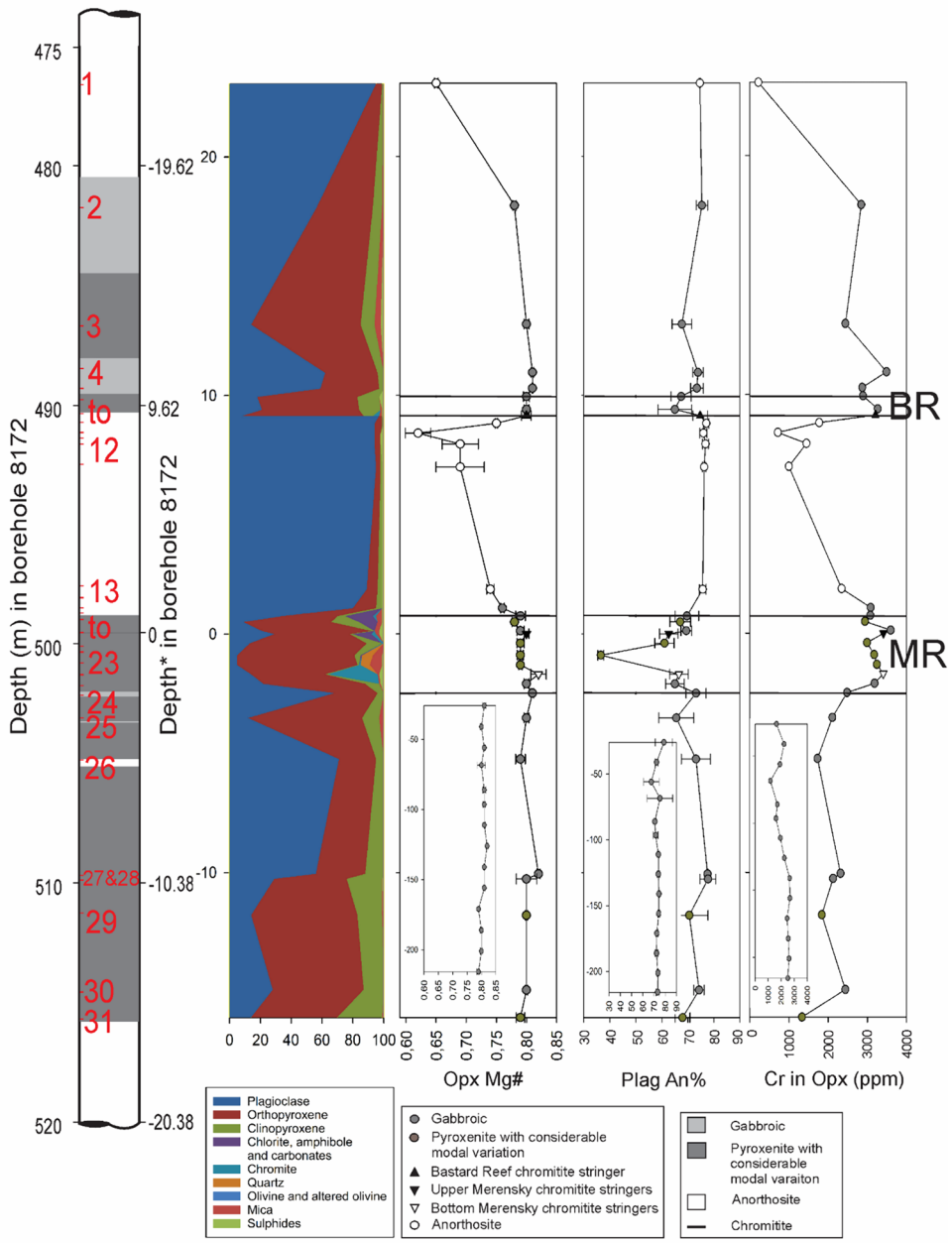


Fig. 7 Simplified lithological log on the left and variation in modal proportions for the depth interval 23.06 m to -16.06 m. Variation in mineral compositions (orthopyroxene Mg#, plagioclase An% and Cr in orthopyroxene) with depth (23.06 m to – 16.06 m) are shown to the right. Error bars indicate 1 standard deviations. *Numbers refer to depth in meters in borehole relative to the top Merensky chromitite stringer. Insets show data for the depth interval -25.96 m to – 215.71 m

samples (Fig. 3a). Wedge-shaped deformation twins and lamellar twinning are commonly encountered. Subhedral to euhedral orthopyroxene crystals (36–78%) are the principal phase within the Merensky Reef interval. Maximum orthopyroxene grain sizes vary from ~ 2 to 5 mm. Clinopyroxene that is typically anhedral and often twinned modally constitutes 1–18% of the Merensky Reef samples. Pleochroic (brown to colourless) amphibole, chlorite and carbonates were noted in abundances ranging between 12 and 18% in three altered samples at depths + 0.75, + 0.5 and 0 m, the latter coinciding with the upper Merensky chromitite stringer. Phlogopite occurs locally within some samples (Fig. 3b) and is abundant in the pyroxenite samples at depths -1.3 and – 0.89 m. Interstitial quartz is also particularly abundant in the two pyroxenite samples (Fig. 3b). Disseminated chromite and sulphides were noted as minor constituents in some samples, with the former occurring as stringers in the samples from depths 0 m and -1.69 m. The upper chromitite stringer is very thin (± 1 mm), with sharp lower and upper contacts. The lower Merensky Reef chromitite stringer (at depth – 1.69 m) has an irregular thickness (± 1 to 15 mm) with chromite occurring almost exclusively as inclusions within apparently intercumulus plagioclase (Fig. 3c), a feature that is not observed at all localities (Smith et al. 2021). In both cases the chromitite stringers consist of chromite that ranges in shape from cubic to amoeboidal. The chromite in

the upper chromitite stringer of the Merensky Reef is dominated by coarser grained chromite (Fig. 3d) compared to the lower chromitite stringer. This is a well-known feature from both the Eastern and Western limbs (Eales and Reynolds 1986 and Mitchell and Scoon 2007). Chromite in the lower chromitite stringer (Fig. 3c) tends to be more rounded and finer grained.

The hangingwall of the Merensky Reef is represented by one leuconorite and 6 anorthosite samples. Plagioclase is the main phase, with a modal abundance of 80–97%. Plagioclase occurs as apparently cumulus, lath-shaped crystals displaying mostly lamellar twinning (Fig. 4a). Orthopyroxene is typically anhedral, modally constitutes 2–15% and is observed most commonly as oikocrysts that enclose plagioclase crystals (Fig. 4a). Plagioclase chadacrysts in the orthopyroxene are small and randomly orientated, compared to the coarser laminated laths, not included in orthopyroxene. Clinopyroxene (1–4%) typically also occurs as oikocrysts enclosing plagioclase (Fig. 4b). Minor fine-grained sulphides occur as small, disseminated grains interspersed between plagioclase crystals.

The Bastard Reef has a sharp basal contact with the underlying mottled anorthosite, with a thin plagioclase-hosted chromitite stringer developed along the contact (Fig. 5a). Chromite within the stringer ranges in shape from cubic to amoeboidal. The reef is represented by a basal pyroxenite sample and two melagabbronorite samples. Orthopyroxene modally constitutes 63–79% of the samples and contains thin and narrowly-spaced clinopyroxene exsolution lamellae. Maximum orthopyroxene grain sizes range between 2 mm and 3.5 mm. Plagioclase (8–21%) appears to be mostly intercumulus and displays wedge-shaped deformation twins and lamellar twinning. It also occurs as inclusions within some orthopyroxene crystals (Fig. 5b). Clinopyroxene containing thick orthopyroxene exsolution lamellae modally constitutes 6–14% of the samples studied. Minor sulphides (1–3%) occur as apparently interstitial phases. Minor phlogopite was additionally noted in two of the samples.

The contact between the Bastard Reef and its hangingwall is poorly defined and gradational. Norite constitutes the lowermost two samples of the hangingwall, followed by melagabbronorite, gabbronorite and finally anorthosite in the uppermost sample collected as part of this study. Orthopyroxene modally constitutes 4–71% of the hangingwall interval and has grain sizes of 2–3 mm. It typically contains thin, narrowly spaced exsolution lamellae of clinopyroxene (Fig. 6a). In the anorthosite, orthopyroxene occurs as oikocrysts enclosing plagioclase chadacrysts (Fig. 6b). Plagioclase modally constitutes 14–95% of the samples studied and occurs as abundantly twinned laths. Wedge-shaped deformation twins and lamellar twinning are common. Anhedral clinopyroxene modally constitutes 0.5–9% of the samples studied. Minor sulphides and brown to colourless pleochroic phlogopite were noted in some samples.

Mineral chemistry

Compositional data for plagioclase, orthopyroxene and clinopyroxene are reported in Electronic Appendix B.6–B.8. The Mg# [molar Mg/(Mg + Fe)] of orthopyroxene in the dominantly gabbroic sequence of rocks below the bottom Merensky chromitite stringer is fairly constant with values between 0.79 and 0.82 (Fig. 7). The Merensky Reef contains orthopyroxene with Mg# values ranging between 0.78 and 0.82, the latter value recorded in the melanorite hosting the basal Merensky chromitite stringer. In the hangingwall to the Merensky Reef, the Mg# of orthopyroxene records a regular decrease from 0.76 in the leuconorite forming the immediate hangingwall to the Merensky Reef, to 0.62 in the mottled anorthosite at depth + 8.41 m. The overlying mottled anorthosite returned a value of 0.75, and the pyroxenite forming the lowermost sample of the Bastard Reef a value of 0.80. Orthopyroxene retains an Mg# value of 0.80–0.81 throughout the Bastard Reef and into its hangingwall up to a depth of + 12.97 m, before decreasing to a value of 0.65 recorded in the uppermost sample collected as part of this study, coincident with the rocks becoming more felsic.

The Mg# of clinopyroxene is on average ~ 0.06 higher than that of the coexisting orthopyroxene. The Mg# of clinopyroxene averages 0.85 in the rocks underlying the Merensky Reef and in the Merensky Reef itself, 0.79 in the hangingwall of the Merensky Reef, 0.85 in the Bastard Reef and 0.84 in the hangingwall of the Bastard Reef.

Several workers (e.g. Eales 2000; Seabrook et al. 2005) have emphasised the difference in Cr in orthopyroxene across the Critical Zone–Main Zone boundary. In the gabbroic rocks underlying the Merensky Reef, the Cr content of orthopyroxene shows very little variation between depths – 215.71 m and – 141.06 m, being on average 2568 ppm (Fig. 7). Values then decrease upwards to a value of 1165 ppm at depth – 68.36 m. A scattered upwards increase follows culminating in a value of 3596 ppm in the melanorite (at depth + 0.13 m) above the upper Merensky chromitite stringer. Values in the Merensky hangingwall are considerably lower, with the lowest value (716 ppm) recorded in the anorthosite at depth + 8.41 m. The overlying Bastard Reef contains orthopyroxene with considerably higher Cr contents, being on average 3076 ppm. Cr in orthopyroxene remains high in the overlying noritic to gabbronoritic rocks, with an average value of 2372 ppm. The lowest Cr in orthopyroxene value was recorded in the overlying anorthosite, having a value of 216 ppm.

The average An% [An% = 100 × molar Ca/(Ca + Na + K)] of plagioclase (Fig. 7) is relatively constant between -215.71 m and -86.04 m, ranging between 70.8 and 74.4, with an

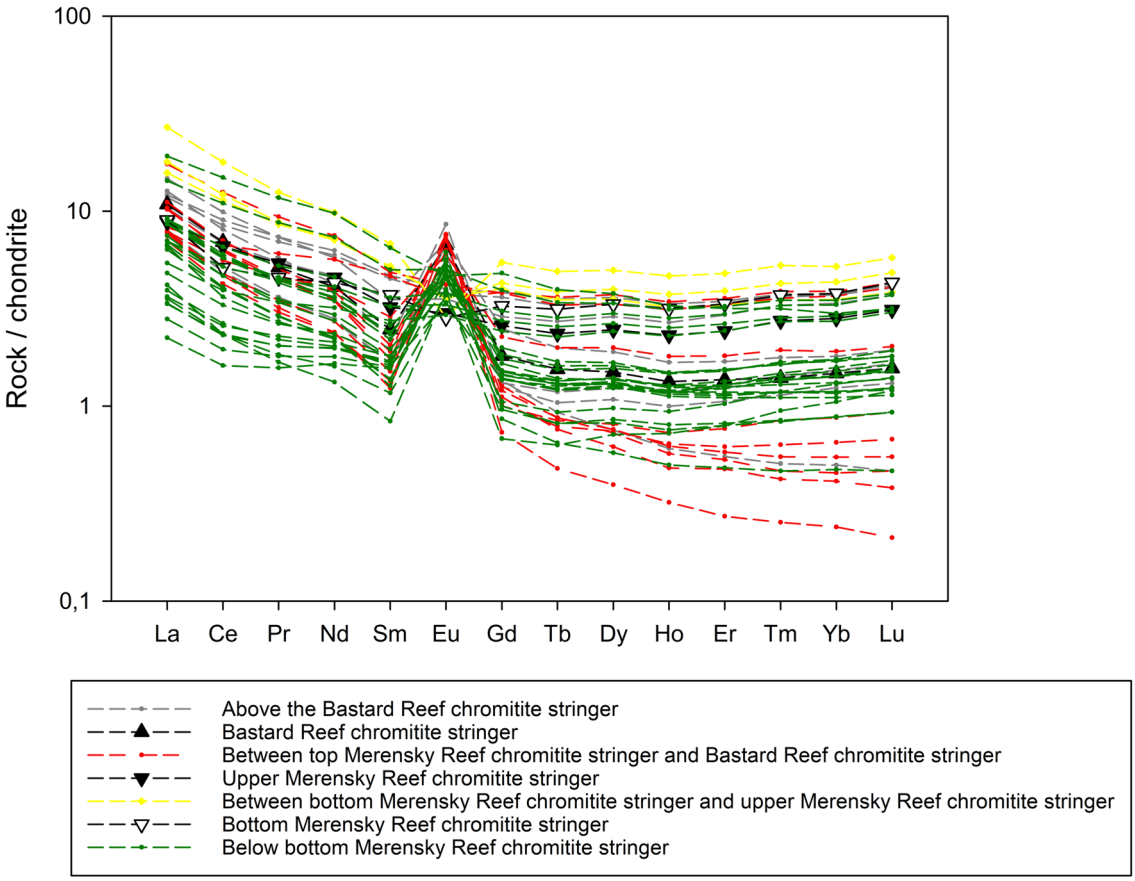


Fig. 8 Chondrite normalized REE patterns of rocks across the Merensky and Bastard reefs as sampled from borehole BH8172. Normalization factors from Lodders (2003)

average value of 73.0 ± 1.2 (1σ). Samples at depths – 68.36 m and – 55.98 m recorded values of 75.3 and 67.6, respectively. A reversal is recorded over the ensuing interval, culminating in a value of 78.8 at depth – 25.96 m. A value of 67.9 is recorded in the melagabbronorite at depth -16.06 m. In the footwall to the Merensky Reef, the An% of plagioclase varies considerably from sample to sample, ranging between 65.5 and 77.7. The An content of the plagioclase of the footwall leuconorite is 73.1 on average. Plagioclase in the Merensky Reef itself is relatively sodic, with an average An% of 65.9 ± 3.2, excluding the anomalously low value of 36.5 encountered in the pyroxenite at depth -0.89. The anorthosite overlying the Merensky Reef has plagioclase with average An% varying between 74.7 and 77.1, the latter value recorded towards the top of the interval. The Bastard Reef contains plagioclase that is more sodic with average An% of 66.2 ± 1.7. The Bastard Reef hangingwall has plagioclase with average An% of 74.3 ± 0.8, excluding that of the melagabbronorite at depth + 12.97 m with a value of 67.7.

Whole-rock major and trace element geochemistry

Whole-rock major and trace element data are reported in Electronic Appendix B.9, B.10. The modal and normative compositions are generally in good agreement, with discrepancies attributable to local sample heterogeneity. Normative An% of plagioclase shows relatively little variation between depths – 215.71 m to – 16.06 m, ranging between 70.3 and 78.6 and scattered about an average value of 74.3. The melagabbronorite at – 14.91 m returned an An% value of 37.5, with values increasing over the ensuing ~ 6.5 m to culminate in a value of 80.1 in the leucogabbronorite at depth – 5.24 m. The melagabbronorite and leuconorite at depths of – 3.52 m and – 2.48 m returned An% values of 63.0 and 75.6, respectively. Normative An% in the Merensky Reef varies considerably from sample to sample, with values ranging from 57.2 to 76.5, with an average value of 68.7 ± 6.2 (1 SD). The leuconorite forming the immediate hangingwall to the Merensky Reef has normative An% of 79.8, with values in the overlying anorthosites ranging between 79.9 and 83.0. Normative An% in the Bastard Reef varies between 62.2 and 77.7. The hangingwall to the Bastard Reef returned values

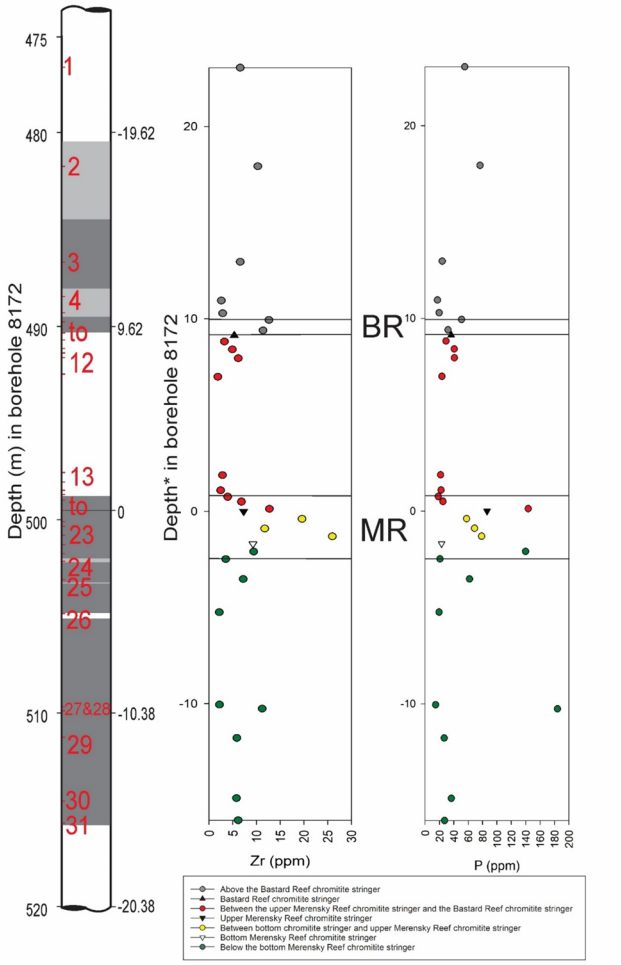


Fig. 9 Variation in whole-rock Zr and P over the depth interval 23.06 m to – 16.06 m

of 64.5–78.7, with a reversal defined by the uppermost three samples of the studied interval.

Whole-rock Mg# is remarkably constant in the sequence of rocks underlying the Merensky Reef, with an average value of 0.83 ± 0.01 (1 SD), and in the Merensky Reef itself, with an average value of 0.82 ± 0.01. Slightly lower Mg#s within the reef may in part be attributable to the presence of sulphides, as observed petrographically and as shown by higher Cu and Ni concentrations in some of the reef samples. In the leuconorite overlying the Merensky Reef, the Mg# is 0.78, with values in the overlying anorthosite decreasing to a low of 0.55 before increasing again to a value of 0.71 in the sample underlying the Bastard Reef. The Bastard Reef itself is considerably more magnesian, with an average Mg# of 0.82. High Mg# values persist in the noritic and gabbroic rocks forming the immediate hangingwall to the Bastard Reef, with an average Mg# value of 0.83. A value of 0.49 was recorded for the anorthosite forming the uppermost sample of the studied interval.

Whole-rock REE data are reported in Electronic Appendix B.11, with chondrite-normalized REE patterns presented in Fig. 8. The majority of the samples exhibit positive europium anomalies ($Eu_N/((Sm_N + Gd_N)/2)$) varying between 1.1 and 7.6. Samples that show negative Eu anomalies or the absence thereof are the pyroxenite and some of the melagabbronorite samples, with values varying between 0.47 and 0.97. All of the samples show enrichment of the LREE relative to the HREE. Samples below the top Merensky chromitite stringer are less enriched in LREE ($Ce/Sm_N = 2.09$ on average) compared to samples between the top Merensky chromitite stringer and the Bastard chromitite stringer with an average Ce/Sm_N of 2.93. Above the Bastard Reef chromitite stringer the Ce/Sm_N decreases again to an average of 2.63. The HREE exhibit an unfractionated pattern below the top Merensky chromitite stringer ($Tb/Yb_N = 1.0$), with a slightly fractionated pattern ($Tb/Yb_N = 1.3$) observed between the top Merensky chromitite stringer and the Bastard Reef. An unfractionated HREE pattern is observed above the Bastard Reef chromitite stringer ($Tb/Yb_N = 1.0$).

Low incompatible element abundances are suggestive of low abundances of trapped melt within most rocks analysed (Fig. 9).

Isotope geochemistry

Whole-rock Sr- and Nd-isotopic data are presented in Table 1, with the variation in depth of $^{87}Sr/^{86}Sr_i$ and ε_{Ndi} displayed graphically in Fig. 10. Samples selected for isotopic analysis were collected mostly from the ~ 40 m interval spanning the Merensky and Bastard reefs, with only a single sample from depth -215.7 m, a gabbronorite, with $^{87}Sr/^{86}Sr_i$ and ε_{Ndi} of 0.7064 and -6.8, respectively. The subsequent sample, from depth – 16.06 m, a melagabbronorite, exhibits $^{87}Sr/^{86}Sr_i$ and ε_{Ndi} values of 0.7067 and – 7.1, respectively. The melagabbronorites underlying the Merensky Reef, at depths of – 10.26 m and – 3.52 m, exhibit $^{87}Sr/^{86}Sr_i$ values of 0.7064 and 0.7070, respectively, with both having ε_{Ndi} of – 6.7. In the Merensky Reef, $^{87}Sr/^{86}Sr_i$ values vary from 0.7064 to 0.7068 (average 0.7065), with ε_{Ndi} of – 7.6 to – 6.3 (average – 6.9). The anorthosite constituting the footwall of the Bastard Reef has $^{87}Sr/^{86}Sr_i$ and ε_{Ndi} values ranging from 0.7071 to 0.7072, and – 6.8 to – 5.9, respectively. The Bastard Reef exhibits $^{87}Sr/^{86}Sr_i$ and ε_{Ndi} values that are indistinguishable from its anorthositic footwall, varying between 0.7071 and 0.7072 for the former, and with ε_{Ndi} from a single sample being – 6.5. Above the Bastard Reef, $^{87}Sr/^{86}Sr_i$ values become progressively more radiogenic, culminating in a value of 0.7077 in the uppermost sample. Values for ε_{Ndi} above the Bastard Reef are scattered between – 6.5 and – 4.9, the latter recorded in the uppermost studied sample.

Table 1 Rb–Sr and Sm–Nd isotopic data for whole-rock samples from BH8172

Depth (m)	Depth* (m)	Rb (ppm)	Sr (ppm)	$^{87}Rb/^{86}Sr$ (measured)	$^{87}Sr/^{86}Sr$ (measured)	$^{87}Sr/^{86}Sr_i$ (2.055 Ga)	Error (2 s)	Nd (ppm)	Sm (ppm)	$^{147}Sm/^{144}Nd$ (measured)	$^{143}Nd/^{144}$ Nd (measured)	$\varepsilon Nd_{i\ (2.055\ Ga)}$	Uncertainty (2 SE)	Lithology
476.56	23.06	2.45	366.89	0.019320	0.708263	0.7077	16	2.29	0.388	0.102544	0.511113	−4.9	0.5	Anorthosite
481.68	17.94	4.09	261.66	0.045220	0.708744	0.7074	30	3.07	0.609	0.119952	0.511269	−6.5	0.3	Gabbronorite
486.65	12.97	1.82	69.08	0.076361	0.709453	0.7072	32	2.25	0.533	0.143092	0.511585	−6.4	0.2	Melagabbronorite
489.68	9.94	3.90	63.02	0.179301	0.712424	0.7071	66	2.87	0.664	0.139689	0.511534	−6.5	0.1	Melagabbronorite
490.22	9.4	4.26	65.20	0.188955	0.712821	0.7072	26	ND	ND	ND	ND	ND	ND	Melagabbronorite
490.48	9.14	2.53	259.44	0.028167	0.707923	0.7071	67	2.33	0.468	0.121381	0.511221	−7.8	0.3	Pyroxenite above and anorthosite below the chromitite stringer
491.21	8.41	2.36	376.17	0.018139	0.707757	0.7072	39	2.17	0.388	0.107926	0.511090	−6.8	0.5	Anorthosite
491.67	7.95	2.23	385.34	0.016761	0.707638	0.7071	52	2.08	0.387	0.112105	0.511193	−5.9	0.5	Anorthosite
498.87	0.75	1.05	266.60	0.011430	0.706861	0.7065	211	2.07	0.493	0.144231	0.511539	−7.6	0.4	Altered melagabbronorite
499.12	0.5	4.46	61.81	0.208817	0.712638	0.7065	13	2.97	0.774	0.157253	0.511762	−6.7	0.2	Altered pegmatoidal pyroxenite
499.49	0.13	10.70	77.13	0.401952	0.718406	0.7065	14	4.10	0.842	0.124292	0.511338	−6.3	0.2	Melanorite
499.62	0	0.61	82.97	0.021300	0.70724	0.7066	52	2.26	0.501	0.134260	0.511437	−7.0	0.2	Altered melanorite
500.01	−0.39	5.65	44.05	0.371436	0.71755	0.7065	92	3.37	0.795	0.142734	0.511556	−6.9	0.2	Melagabbronorite
500.51	−0.89	9.30	63.95	0.421218	0.71887	0.7064	12	3.46	0.782	0.136754	0.511497	−6.5	0.2	Pyroxenite
500.92	−1.3	ND	ND	ND	ND	ND	ND	4.87	1.043	0.129323	0.511375	−6.9	0.2	Pyroxenite
501.31	−1.69	ND	ND	ND	ND	ND	ND	2.13	0.578	0.163983	0.511840	−7.0	0.3	Melanorite
501.71	−2.09	4.29	111.80	0.111100	0.7101	0.7068	33	3.64	0.789	0.131071	0.511386	−7.1	0.2	Pegmatoidal Melagabbronorite
503.14	−3.52	1.64	78.53	0.060510	0.708762	0.7070	97	2.35	0.568	0.146041	0.511611	−6.7	0.2	Melagabbronorite
509.88	−10.26	8.99	104.39	0.249234	0.713804	0.7064	24	5.08	1.086	0.129234	0.511381	−6.7	0.2	Melagabbronorite

Table 1 (continued)

Depth (m)	Depth* (m)	Rb (ppm)	Sr (ppm)	$^{87}Rb/^{86}Sr$ (measured)	$^{87}Sr/^{86}Sr$ (measured)	$^{87}Sr/^{86}Sr_i$ (2.055 Ga)	Error (2 s)	Nd (ppm)	Sm (ppm)	$^{147}Sm/^{144}Nd$ (measured)	$^{143}Nd/^{144}Nd$ (measured)	$\varepsilon Nd_{i\ (2.055\ Ga)}$	Uncertainty (2 SE)	Lithology
515.68	−16.06	1.28	63.07	0.058722	0.708375	0.7066	61	1.93	0.491	0.153422	0.511688	−7.1	0.3	Melagabbronorite
715.33	−215.71	2.49	218.05	0.033059	0.707382	0.7064	23	1.86	0.403	0.130776	0.511397	−6.8	0.2	Gabbronorite

2 SE uncertainties on initial isotope ratios include uncertainties propagated from measured isotope ratios

ND No data

Discussion

The variation in whole-rock major element compositions is controlled by and large by variations in the modal abundance of the main silicate phases present, viz. plagioclase, orthopyroxene and clinopyroxene (Electronic Appendix A.2). Low trace element abundances (Fig. 9, Fig. 11a) suggest that most rocks examined are adcumulates. Higher amounts of trapped melt are observed mainly in some Merensky Reef samples, with Ce/Sm ratios supporting a B1 + B2, Critical Zone parentage, in line with previous suggestions to this effect (Eales et al. 1990; Barnes et al. 2010) (Fig. 11b).

Nd-isotopic compositions

The results of our Nd-isotopic study (see Fig. 10) turned out to be somewhat ambiguous, largely due to the dearth of available Nd-isotopic data on the Bushveld Complex. The sample with the highest $^{87}Sr/^{86}Sr_i$ ratio, being the uppermost sample collected as part of this study, and presumably representing the sample with the highest contribution from the Main Zone magma, also has the most radiogenic Nd-isotopic composition ($\varepsilon_{Ndi} = -4.9$). The lowermost sample collected as part of this study, and presumably representing the sample with the highest contribution from the Critical Zone magma, at least based on its stratigraphic position, has an ε_{Ndi} value of -6.8. Maier et al. (2000) showed the opposite, with rocks of the Lower and Lower Critical Zones exhibiting more radiogenic Nd-isotopic compositions compared to the Upper Critical and Main zones. Their study was, however, based only on 2 Lower Zone, 3 Lower Critical Zone, 8 Upper Critical Zone and 4 Main Zone samples. Taken in isolation, the present results may suggest that the magma responsible for the formation of the lower Main Zone was more radiogenic than that of the Critical Zone. Keet et al. (2024) showed a similar trend of ε_{Ndi} values becoming more radiogenic upwards above the Upper Reef, being the correlate of the Bastard Reef in the Flatreef of the Northern Limb of the Bushveld Complex. Proper contextualisation of the present results would necessitate a larger Nd-isotopic database, particularly for the lower Main Zone.

Mineral disequilibrium across the Merensky-Bastard interval

Sr-isotopic data from the present study across the Merensky-Bastard interval are consistent with the data obtained at numerous sites on both the Eastern (Lee and Butcher 1990; Seabrook et al. 2005) and Western (Kruger and Marsh 1982; Eales et al. 1990; Kruger 1992) limbs, with the interval recording an upward increase from "typical" Upper Critical Zone initial $^{87}Sr/^{86}Sr$ ratios on the order

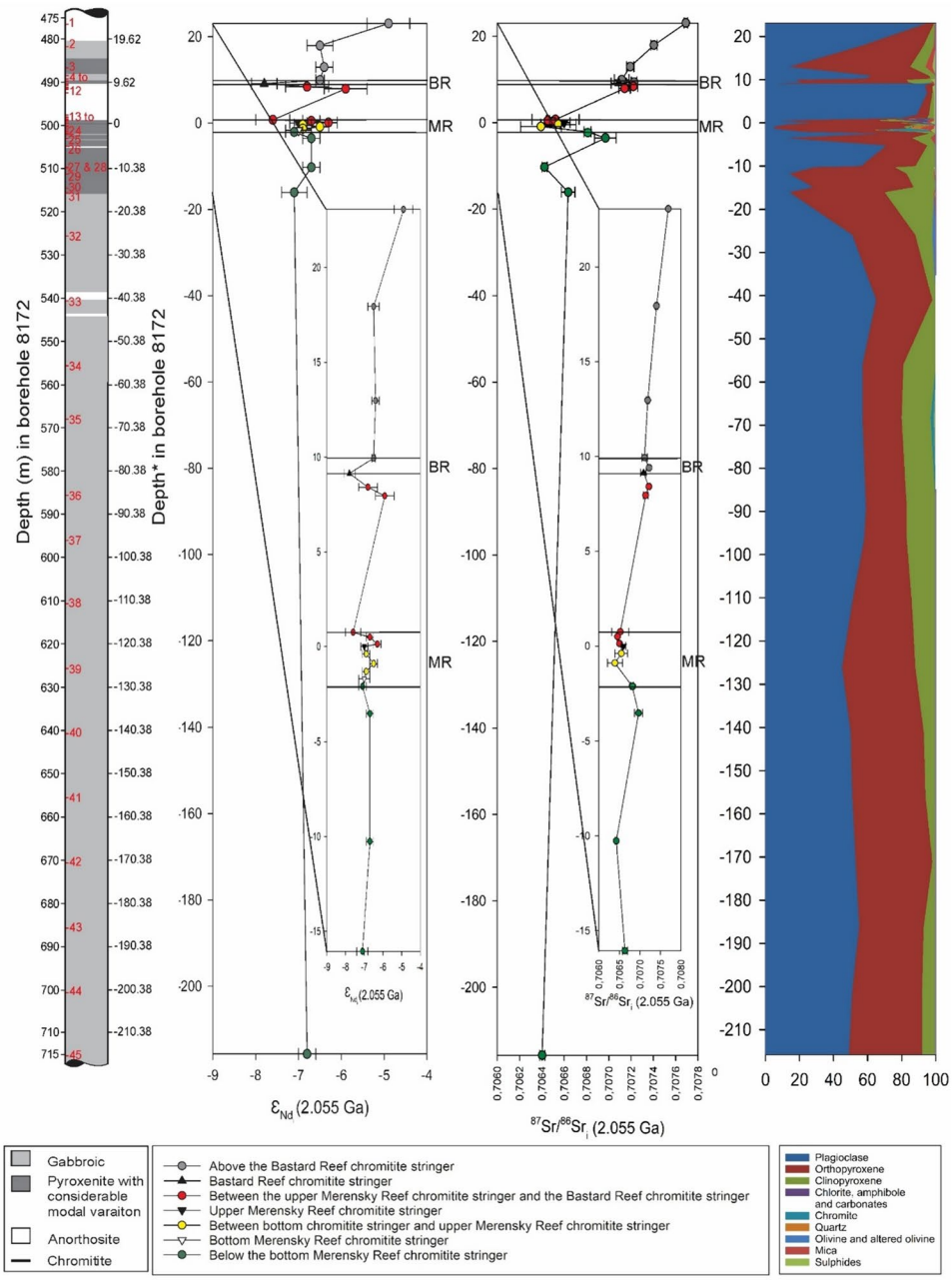


Fig. 10 Variations in ε_{Ndi} (at 2.055 Ga) and $^{87}Sr/^{86}Sr_i$ (at 2.055 Ga) with depth across the Bastard Reef – Merensky Reef interval in BH8172. Error bars show 2 SE. *Numbers refer to depth in meters in borehole relative to the base of the upper Merensky Reef chromitite stringer. Insets show close-ups of the area around the Merensky and Bastard reef chromitite stringers

of 0.7060–0.7068 in the footwall of the Merensky Reef, to "typical" Lower Main Zone values > 0.7075 above the Bastard Reef (Seabrook et al. 2005) (Fig. 12). Our data are also consistent with the notion that the Merensky-Bastard interval represents an interval hosting rocks that formed through the co-accumulation of minerals from compositionally and isotopically distinct magmas, as has been argued by Prevec et al. (2005) and Seabrook et al. (2005).

Seabrook et al. (2005) indicated that it was possible to use whole-rock geochemical data, specifically Sr-isotopic compositions and Cr/MgO ratios, to distinguish from which magma (i.e. Critical Zone or Main Zone) a particular mineral occurring within rocks of the Merensky-Bastard interval was derived. Whole-rock Cr/MgO was used as a proxy for orthopyroxene, with rocks exhibiting ratios between 80 and 120 containing orthopyroxene derived from the Critical Zone magma, and rocks exhibiting ratios < 60 being derived from the Main Zone magma. Whole-rock $^{87}Sr/^{86}Sr_i$ was used as a proxy for plagioclase, with rocks exhibiting values < 0.7068 containing plagioclase derived from the Critical Zone magma, and rocks exhibiting values > 0.7075 being derived from the Main Zone magma. The relevant data from our study are presented graphically in Fig. 13.

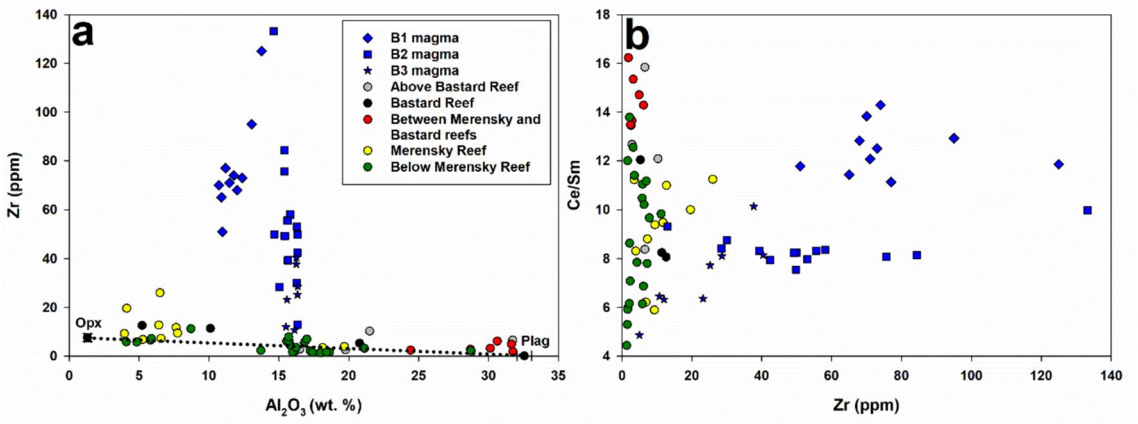


Fig. 11 **a** Variation in whole-rock Zr with Al_2O_3 and **b** Ce/Sm with Zr in rocks occurring across the Merensky-Bastard interval, compared with that of the suite of marginal rocks. Compositions of the latter come from Barnes et al. (2010). Orthopyroxene (in pyroxenite) and plagioclase (in anorthosite) compositions are from Veksler et al. (2015)

Using the proposed values of Seabrook et al. (2005), our data indicate that the Merensky Reef and its footwall host both orthopyroxene and plagioclase derived from the Critical Zone magma, excluding a single footwall sample exhibiting a mixed signature. Data are available for only two samples from the noritic to anorthositic interval between the Merensky and Bastard reefs. The lower sample contains both plagioclase and orthopyroxene with a mixed parentage, whereas the upper sample contains plagioclase with a mixed parentage, and orthopyroxene that apparently originated only from within the Main Zone magma. The Bastard Reef and its immediate hanging wall contains orthopyroxene with a clear Critical Zone affinity and plagioclase with a mixed Critical Zone–Main Zone affinity. The uppermost sample analysed as part of this study appears to consist of both orthopyroxene and plagioclase derived solely from the Main Zone magma.

Seabrook et al. (2005), having examined the Southern Sector of the Eastern Limb at Richmond, suggested that Main Zone magma intruded at the approximate level of the Merensky Reef, elevating the residual Critical Zone magma. Orthopyroxene (± plagioclase) that crystallised in the elevated Critical Zone magma settled through the underlying Main Zone magma and accumulated on the immediate floor of the chamber to form the Merensky Reef. The noritic to anorthositic hanging wall of the Merensky Reef then crystallised largely from the Main Zone magma, with additional input of orthopyroxene derived from the overlying Critical Zone magma. A second pulse of orthopyroxene crystallisation in the Critical Zone magma led to the development of the Bastard Reef, that incorporated interstitial plagioclase from the Main Zone magma or cumulus plagioclase derived from the Critical Zone magma.

An alternative model for the petrogenesis of the Merensky-Bastard interval

Seabrook et al. (2005), using compositional data of Li et al. (2001) and Cawthorn et al. (1981) and the equations of Bottinga and Weill (1970), show convincingly that the Main Zone magma was denser (2.71 g/cm^{-3}) than the Critical Zone magma (2.59 g/cm^{-3}), confirming the earlier work of Hatton (1989). They also cite Campbell (1978), who reported the density of plagioclase as 2.7 g/cm^{-3} at a temperature that could reasonably be expected for the Main Zone magma. Somewhat inexplicably, they argue that the plagioclase had a density close to that calculated for the Main Zone magma and that plagioclase would therefore have settled from the magma along with orthopyroxene. A possibility that was never considered is whether plagioclase, being somewhat less dense than the Main Zone magma, would have floated rather than settled from the magma.

The question as to whether plagioclase floated or settled within the context of the Bushveld Complex has been addressed by several workers. Cawthorn and Ashwal (2009) found no evidence to support flotation of plagioclase in the upper reaches of the Rustenburg Layered Suite, noting the depletion in plagioclase relative to its cotectic proportions in the uppermost 100 m of the intrusion. Cawthorn (2002) suggested that plagioclase accumulation may have been delayed within the Upper Critical Zone despite the magma being saturated in both orthopyroxene and plagioclase, with plagioclase remaining in suspension (but not floating), whilst orthopyroxene settled. Flotation of plagioclase is considered an important process in the generation of Proterozoic massif-type anorthosites (Ashwal 1993) and has also been suggested to have occurred within putative sub-Bushveld

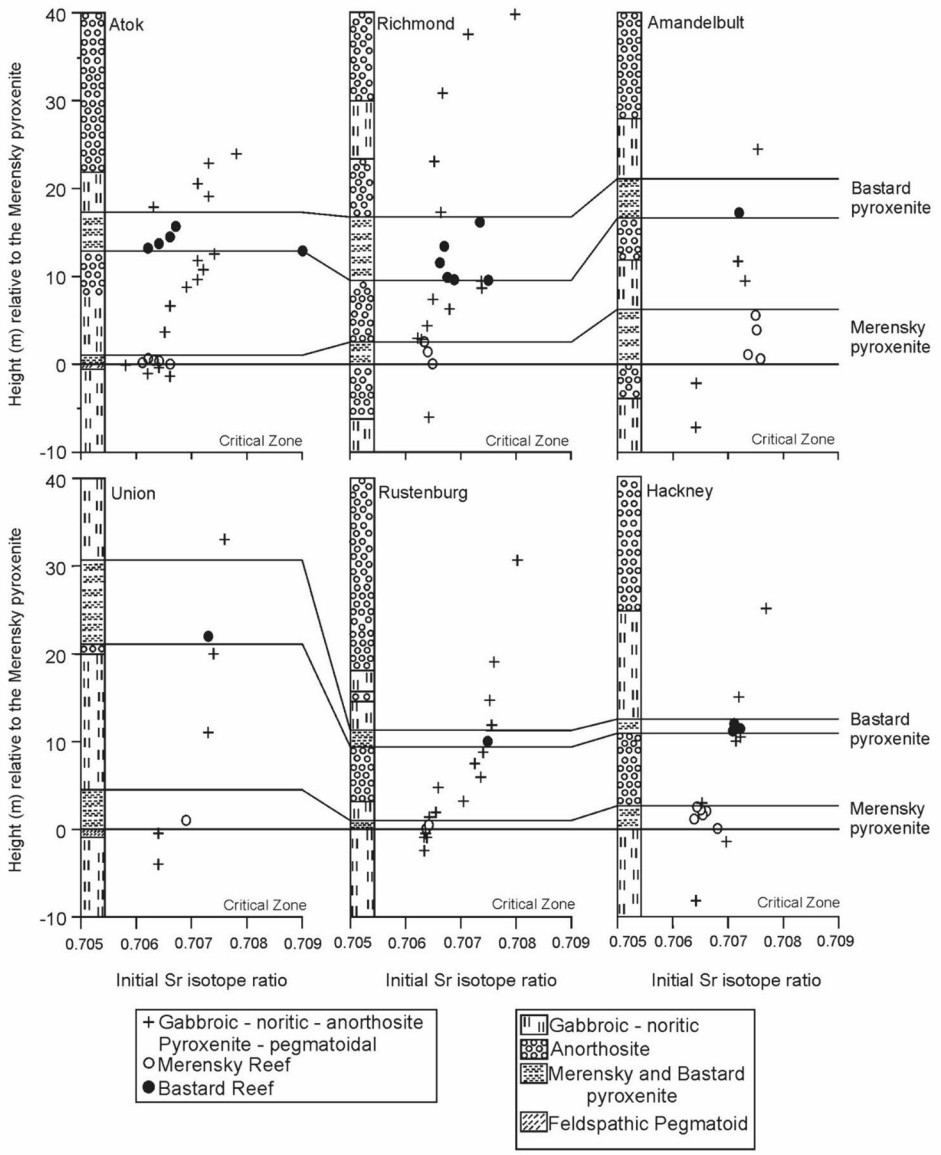


Fig. 12 Variation in $^{87}Sr/^{86}Sr$ across the Merensky-Bastard interval at Hackney (this study), Atok (Lee & Butcher 1990), Richmond (Seabrook et al. 2005), Amandelbult (Kruger 1992), Union (Eales et al. 1990) and Rustenburg (Kruger & Marsh 1982)

magma chambers (Roelofse and Ashwal 2012; Roelofse et al. 2015), the existence of which has recently been confirmed geophysically (Cole et al. 2024). In the context of the Merensky-Bastard interval specifically, Vermaak (1976) suggested that the flotation of plagioclase was responsible for the formation of anorthositic layers in cyclic units both above and below the Merensky Reef, citing in support the commonly encountered upward increase in the anorthite content of plagioclase towards the upper reaches of the anorthosite layers, a feature also noted in the anorthositic sequence beneath the Bastard Reef in our study.

The model of Vermaak (1976) does not appear to have garnered much support in the more recent literature, despite explaining several features of the Merensky-Bastard interval, including aspects of our own dataset. We propose that the noritic to anorthositic interval between the Merensky and Bastard reefs may have formed in response to the injection of a plagioclase-laden pulse of Main Zone magma, but that plagioclase floated instead of settled from this magma. The following sequence of events, shown graphically in Fig. 14, is suggested to explain our observations on the interval that we studied:

(i) A pulse of magma with a Critical Zone affinity enters the chamber as a basal flow, causing chamber-wide erosion along the chamber floor (Fig. 14a). The magma crystallises orthopyroxene that accumulates or grows in-situ to form the Merensky Reef (Fig. 14b). Whole-rock Sr-isotopic compositions and Cr/MgO ratios as shown in Fig. 13 indicate that the Merensky Reef con-

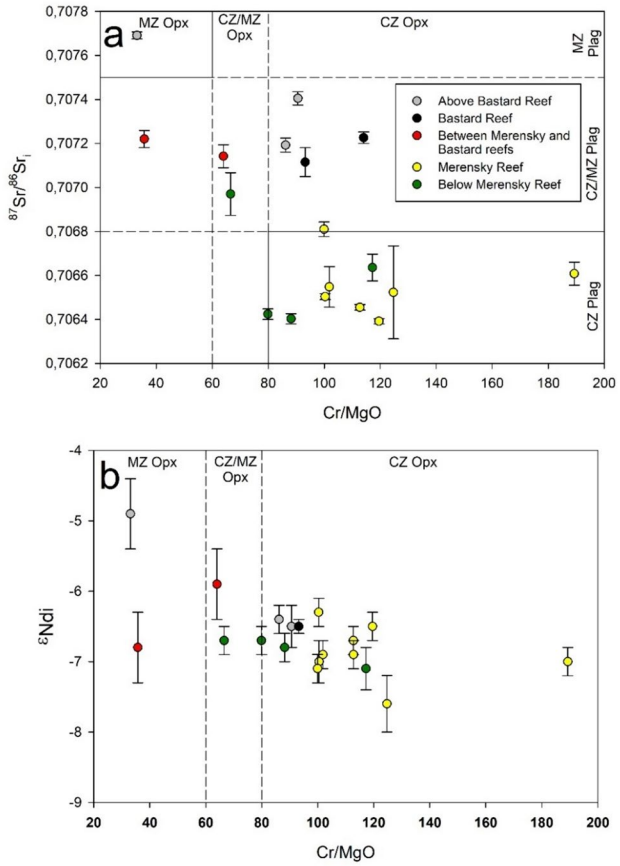


Fig. 13 Variation in **a** whole-rock Cr/MgO vs $^{87}Sr/^{86}Sr_i$ and **b** Cr/MgO vs ε_{Ndi} for rocks occurring across the Merensky-Bastard interval as sampled by borehole BH8172. See text for details. Error bars show 2 SE. Cr in ppm and MgO as wt%

tains both plagioclase and orthopyroxene with a distinctly Critical Zone parentage.

(ii) A plagioclase-laden pulse of Main Zone magma enters the chamber, elevating the resident Critical Zone magma (Fig. 14c). The newly added magma causes localised erosion of the upper reaches of the Merensky Reef. It is envisaged that the magma entered as a constant-flux gravity current (Hallworth et al. 1996), potentially from multiple irruptive centres (*cf.* Eales et al. 1988), and that mixing and entrainment of resident magma into this influx was minimal.

(iii) Plagioclase (density = 2.7 g/cm^{-3}) within this layer floats as it is less dense than the magma (density = 2.71 g/cm^{-3}) in which it occurs. The plagioclase accumulates along the interface between the intruded Main Zone magma and the displaced Critical Zone magma (density = 2.59 g/cm^{-3}) (Fig. 14d). Very limited mixing (*cf.* Irvine 1977) occurs along this interface, resulting in the formation of the very thin chromitite layer marking the base of the Bastard Reef (see Fig. 5a). The reversal in plagioclase An% recorded in the anorthositic interval between the Merensky and Bastard reefs (Fig. 7) is consistent with the flotation of plagioclase.

(iv) The floated plagioclase solidifies, forming an anorthositic raft on which orthopyroxene derived from the Critical Zone accumulates to form the Bastard Reef. Contemporaneously, the Main Zone magma underlying the anorthositic raft crystallises forming the leuconoritic hanging wall of the Merensky Reef (Fig. 14e). The Bastard Reef has a Cr/MgO ratio suggesting derivation of the orthopyroxene that it contains from the Critical Zone magma. Upward infiltration of melt from the solidifying anorthosite raft is thought to be responsible for the elevated $^{87}Sr/^{86}Sr_i$ values observed in the Bastard Reef, a process that also explains the apparently low amounts of trapped melt in the interval between the Merensky and Bastard reefs (Fig. 11).

(v) Subsequent additions of Main Zone magma to the chamber above the level of the Bastard Reef resulted in the deposition of rocks with Sr-isotopic compositions that become progressively more radiogenic with height across the Giant Mottled Anorthosite interval and into the lower Main Zone (Fig. 14f), as shown by Kruger (1994).

Implications for the PGE budget of the Merensky Reef

Our suggestion that the bulk of the magma present in the chamber was separated from the Merensky Reef by a solid layer of anorthosite onto which the Bastard Reef was deposited would imply that the Main Zone could not have been the source of the PGEs present within the Merensky Reef. The upward increase in the Pt + Pd concentrations of chromitite layers throughout the Critical Zone, which culminates in the Merensky Reef (Scoon and Teigler 1994), therefore likely reflects a pre-emplacement evolutionary trend that is consistent with the "off-stage" school of thought as explained above.

Conclusions

Our data across the Merensky-Bastard interval at Hackney are consistent with the results of previous studies that argued for the co-accumulation of minerals from compositionally and isotopically distinct magmas, of Critical and Main Zone lineages, respectively, across this interval. Previous studies, like that of Seabrook et al. (2005), suggested that accumulation of plagioclase and orthopyroxene across this interval occurred through settling, without considering the

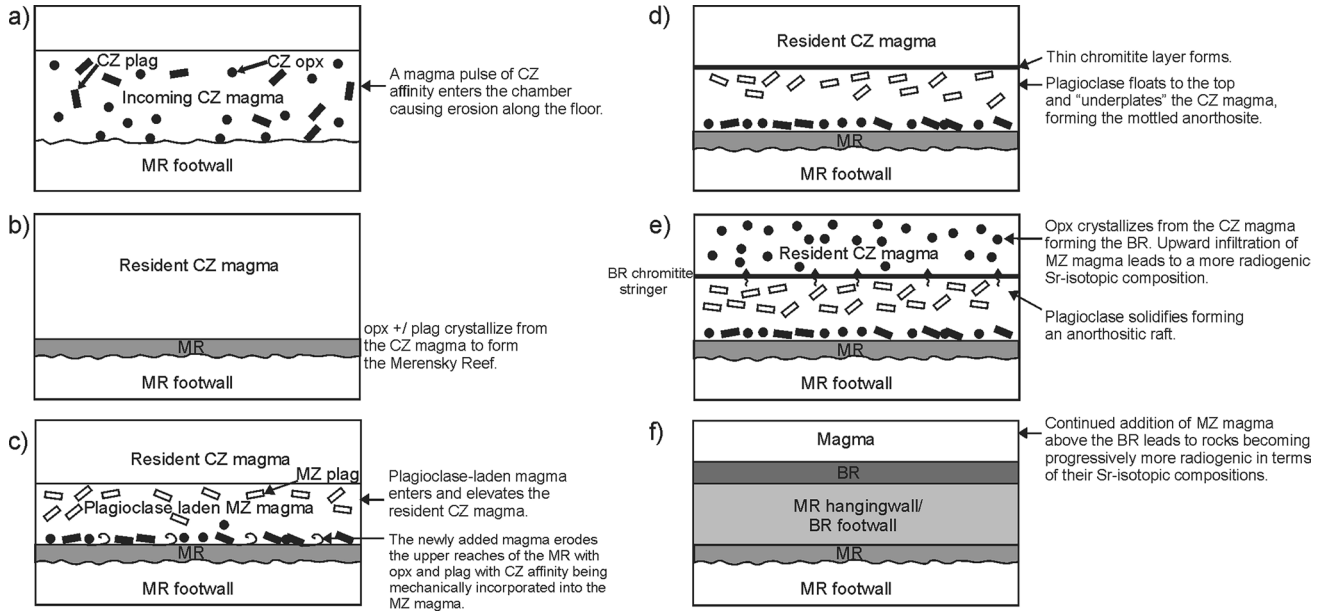


Fig. 14 Schematic representation of the proposed sequence of events responsible for the formation of the Merensky-Bastard interval. See text for details. *MR* Merensky Reef, *BR* Bastard Reef, *MZ* Main Zone, *CZ* Critical Zone, *plag* plagioclase, *opx* orthopyroxene

possibility that plagioclase may have floated (*cf.* Vermaak 1976), despite citing densities of plagioclase and Main Zone magma that would have resulted in plagioclase floating. In our model, the Bastard Reef was deposited from an upper, elevated layer of Critical Zone magma, onto a plagioclase raft that floated on a layer of Main Zone magma overlying the Merensky Reef, a model that is entirely consistent with density considerations as per Seabrook et al. (2005). From a metallogenetic viewpoint, this implies that the Main Zone could not have been the source of the PGEs present within the Merensky Reef.

Supplementary Information The online version contains supplementary material available at https://doi.org/10.1007/s00410-024-02155-8.

Acknowledgements The authors would like to thank Kimberley Beaton, Karen Smit (University of the Witwatersrand) and Henriette Ueckermann (University of Johannesburg) for their help with the isotopic analyses. We thank Marlin Patchappa and Allan Wilson (Earth Observatory at the University of the Witwatersrand) and Mrs Megan Purchase (University of the Free State) for assistance with geochemical analyses. Constructive reviews by Stephen Barnes, Ilya Veksler and an anonymous reviewer and the editorial handling by Dante Canil are gratefully acknowledged. This work was funded in part by CIMERA (DSI-NRF Centre of Excellence for Integrated Mineral and Energy Resource Analysis) and the NRF (National Research Foundation). Funding is also acknowledged through NRF-NEP grant (UID 129777) to Robert Bolhar and Grant Bybee to establish the MC-ICPMS and TIMS facility at the University of the Witwatersrand. Any finding, opinions and conclusions expressed are those of the authors and the NRF and CIMERA do not accept any liability.

Funding Open access funding provided by University of the Free State. DSI-NRF Centre of Excellence for Integrated Mineral and Energy Resource Analysis, National Research Foundation, 129777, 129777, Grant Bybee.

Data availability Information regarding the availability of the research data has been added to the "Supplementary Material" section.

Open Access This article is licensed under a Creative Commons Attribution 4.0 International License, which permits use, sharing, adaptation, distribution and reproduction in any medium or format, as long as you give appropriate credit to the original author(s) and the source, provide a link to the Creative Commons licence, and indicate if changes were made. The images or other third party material in this article are included in the article's Creative Commons licence, unless indicated otherwise in a credit line to the material. If material is not included in the article's Creative Commons licence and your intended use is not permitted by statutory regulation or exceeds the permitted use, you will need to obtain permission directly from the copyright holder. To view a copy of this licence, visit http://creativecommons.org/licenses/by/4.0/.

References

Ashwal LD (1993) Anorthosites in layered mafic intrusions. Miner Rocks Ser 21:219–261

Ashwal LD, Webb SJ, Knoper MW (2005) Magmatic stratigraphy in the Bushveld Northern Lobe: continuous geophysical and mineralogical data from the 2950m Bellevue drill core. S Afr J Geol 108:199–232

Barnes S-J, Maier WD, Curl EA (2010) Composition of the Marginal rocks and sills of the Rustenburg layered suite, Bushveld Complex, South Africa: implications for the formation of the platinum-group element deposits. Econ Geol 105:1491–1511

Begemann F, Ludwig KR, Lugmair GW, Min K, Nyquist LE, Patchett PJ, Renne PR, Shih Y, Villa IM, Walker RJ (2001) Call for an improved set of decay constants for geochronological use. Geochimica Et Cosmochemica Acta 65:111–121

Beukes JJ, Roelofse F, Gauert CDK, Grobler DF, Ueckermann H (2021) Strontium isotope variations in the Flatreef on Macalacaskop, northern limb, Bushveld Complex: implications for the source of platinum-group elements in the Merensky Reef. Miner Deposita 56(4):45–57

Bottinga Y, Weill DF (1970) Densities of liquid silicate systems calculated from partial molar volumes of oxide components. Am J Sci 269:169–182

Boudreau AE, McCallum IS (1992) Infiltration metasomatism in layered intrusions – an example from the Stillwater Complex, Montana. J Volcanol Geoth Res 52:171–183

Bouvier A, Vervoort JD, Patchett PJ (2008) The Lu-Hf and Sm-Nd isotopic composition of CHUR: constraints from unequilibrated chondrites and implications for the bulk composition of terrestrial planets. Earth Planet Sci Lett 273(1–2):48–57

Cameron EN, Abendroth HE (1957) Structure of lopoliths: discussion. Bull Geol Soc s. Afr 79:3–12

Campbell IH (1978) Plagioclase buoyancy in basaltic liquids as determined with a centrifuge furnace. Contrib Miner Petrol 67:369–377

Campbell IH, Naldrett AJ, Barnes SJ (1983) A model for the origin of platinum-rich sulphide horizons in the Bushveld and Stillwater complexes. J Petrol 24:133–165

Cawthorn RG (1999) Permeability of the footwall cumulates to the Merensky Reef, Bushveld Complex: South African. J Geol 102:268–281

Cawthorn RG (2002) Delayed accumulation of plagioclase in the Bushveld Complex. Mineral Mag 66(6):881–893

Cawthorn RG (2005) Pressure fluctuations and the formation of the PGE-rich Merensky and chromitite reefs, Bushveld Complex. Miner Deposita 40:231–235

Cawthorn RG (2010) The platinum group element deposits of the Bushveld Complex in South Africa. Platin Met Rev 54(4):205–215

Cawthorn RG (2011) Geological interpretations from the PGE distribution in the Bushveld Merensky and UG2 chromitite reefs. J S Afr Inst Min Metall 111:67–79

Cawthorn RG, Ashwal LD (2009) Origin of anorthosite and magnetitite layers in the Bushveld Complex, constrained by major element compositions of plagioclase. J Petrol 50(9):1607–1637

Cawthorn RG, Boerst K (2006) Origin of the pegmatitic pyroxenite in the Merensky unit, Bushveld Complex, South Africa. J Petrol 47(8):1509–1530

Cawthorn RG, Davies G, Clubley-Armstrong A, McCarthy TS (1981) Sills associated with the Bushveld Complex, South Africa: an estimate of parental magma composition. Lithos 14:1–15

Cole J, Finn CA, Webb SJ (2024) Deep magmatic staging chambers for crustal layered intrusions: an example from the Bushveld Complex of southern Africa. Precambr Res 403:1–10

Eales HV (2000) Implications of the chromium budget of the Western limb of the Bushveld Complex. S Afr J Geol 103(2):141–150

Eales HV, Cawthorn RG (1996) The Bushveld Complex. In: Cawthorn RG (ed) Layered intrusions. Elsevier Science, Amsterdam, pp 181–229

Eales HV, Costin G (2012) Crustally contaminated Komatiite: primary source of the chromitites and marginal, lower and critical zone magmas in a staging chamber beneath the Bushveld Complex. Econ Geol 107:645–665

Eales HV, Reynolds IM (1986) Cryptic variations within chromitites of the upper critical zone, northwest Bushveld Complex. Econ Geol 81:1056–1066

Eales HV, Marsh JS, Mitchell AA, de Klerk WJ, Kruger FJ, Field M (1986) Some geochemical constraints upon models for the crystallization of the upper critical zone – main zone interval, northwestern Bushveld Complex. Mineral Mag 50:567–582

Eales HV, Field M, De Klerk WJ, Scoon RN (1988) Regional trends of chemical variations and thermal erosion in the upper critical zone, Western Bushveld Complex. Mineral Mag 52:63–79

Eales HV, de Klerk WJ, Teigler B (1990) Evidence for magma mixing processes within the critical and lower zones of the northwestern Bushveld Complex, South Africa. Chem Geol 88:261–278

Goldstein SL, O'Nions RK, Hamilton PJ (1984) A Sm-Nd study of atmospheric dusts and particulates from major river systems. Earth Planet Sci Lett 70:221–236

Grobler DF, Brits JAN, Maier WD, Crossingham A (2019) Litho-and chemostratigraphy of the Flatreef PGE deposit, northern Bushveld Complex. Miner Deposita 54:3–28

Hallworth MA, Huppert HE, Phillips JC, Sparks SJ (1996) Entrainment into two-dimensional and axisymmetrix turbulent gravity currents. J Fluid Mech 308:289–311

Hatton CJ (1989). Densities and liquidus temperatures of Bushveld parental magmas as constraints on the formation of the Merensky reef of the Bushveld Complex, South Africa. In: Prendergast, M.D., and Jones M.J., eds., UK, Institution for Mining and Metallurgy, p. 87–93.

Hunt E, Latypov R, Horvath P (2018) The Merensky cyclic unit, Bushveld Complex, South Africa: reality or a myth? Minerals 8:144

Hunter RH (1987) Textural equilibrium in layered igneous rocks. In: Parsons I (ed) Origins of igneous layering. Reidel, Dordrecht, pp 473–503

Hutchinson D, Foster J, Prichard H, Gilbert S (2015) Concentration of particulate platinum-group minerals during magma emplacement: a case study from the Merensky Reef, Bushveld Complex. J Petrol 56:113–159

Irvine TN (1977) Origin of chromitite layers in the Muskox intrusion and other layered intrusions: a new interpretation. Geology 5:273–277

Jacobsen SB, Wasserburg GJ (1980) Sm-Nd isotopic evolution of chondrites. Earth Planet Sci Lett 50:139–155

Karykowski BT, Yang SH, Maier WD, Lahaye Y, Lissenberg CJ, O'Brien H (2017) In situ Sr isotope compositions of plagioclase from a complete stratigraphic profile of the Bushveld Complex, South Africa: evidence for extensive magma mixing and percolation. J Petrol 58(11):2285–2308

Keet JJ, Roelofse F, Gauert CDK, Grobler D, Butler M (2021) A comparative study of sulfur isotope variations within the Flatreef and Merensky Reef of the Bushveld Complex, South Africa. Canadian Mineralogy 59:1363–1380

Keet JJ, Roelofse F, Gauert CDK, Iaccheri LM, Grobler DF, Ueckermann H (2024) Neodymium isotope variations in the Flatreef on Macalacaskop, northern limb, Bushveld Complex. Miner Deposita 59:275–290

Kinnaird JA, Kruger FJ, Nex PAM, Cawthorn RG (2002) Chromite formation- a key to understanding processes of platinum enrichment. Trans Inst Min Metall 111:B23–B35

Kruger FJ (1990) The stratigraphy of the Bushveld Complex: a reappraisal and the relocation of the main zone boundaries. S Afr J Geol 92:376–381

Kruger FJ (1992) The origin of the Merensky cyclic unit: Sr-isotopic and mineralogical evidence for an alternative orthomagmatic model. Aust J Earth Sci 39:255–261

Kruger FJ (1994) The Sr-isotopic stratigraphy of the western Bushveld Complex. S Afr J Geol 97:393–398

Kruger FJ, Marsh JS (1982) Significance of $^{87}Sr/^{86}Sr$ ratios in the Merensky cyclic unit of the Bushveld Complex. Nature 298:53–55

Kruger FJ (2010) The Merensky and bastard cyclic units and platreef of the bushveld complex: consequences of main zone magma influxes and dynamics. The 4th international platinum conference, platinum in transition 'Boom or Bust'. Southern Africa institute of mining and metallurgy, Johannesburg, South Africa, p. 43–46.

Latypov R, Chistyakova S, Page A, Hornsey R (2015) Field evidence for the in situ crystallization of the Merensky Reef. J Petrol 56:2341–2372

Latypov R, Chistyakova S, Kramers J (2017) Arguments against synmagmatic sills in the Bushveld Complex, South Africa. S Afr J Geol 120(4):565–574

Latypov R, Chistyakova S, Kramers J (2018) Reply to discussion of "Arguments against synmagmatic sills in the Bushveld Complex, South Africa" by Roger Scoon and Andrew Mitchell. S Afr J Geol 121(2):211–216

Lee CA, Butcher AR (1990) Cyclicity in the Sr isotope stratigraphy through the Merensky reef and Bastard reef units, Atok section, eastern Bushveld Complex. Econ Geol 85:877–883

Li C, Maier W, de Waal SA (2001) The role of magma mixing in the genesis of PGE mineralization in the Bushveld Complex: Thermodynamic calculations and new interpretations. Econ Geol 96:653–662

Lodders K (2003) Solar system abundances and condensation temperatures of the elements. Astrophys J 591:1220–1247

Luu T, Gutiérrez P, Inglis EC, Chauvel C, Roberts DJ (2022) High-precision Sr and Nd isotope measurements using a dynamic zoom lens- equipped thermal ionisation mass spectrometer. Chem Geol 611:121078

Magson J, Roelofse F, Bybee G, Bolhar R (2023) Constraints on the Nd-isotopic composition and nature of the last major influx of magma into the Bushveld Complex. Contrib Miner Petrol 178:14

Maier WD, Arndt NT, Curl EA (2000) Progressive crustal contamination of the Bushveld Complex: evidence from Nd isotopic analyses of the cumulate rocks. Contrib Miner Petrol 140:316–327

Maier WD, Barnes SJ, Groves DI (2013) The Bushveld Complex, South Africa: formation of platinum-palladium, chrome- and vanadium-rich layers via hydrodynamic sorting of a mobilised cumulate slurry in a large, relatively slowly cooling, subsiding magma chamber. Miner Deposita 48:1–56

Mathez EA, Hunter RH, Kinzler R (1997) Petrologic evolution of partially molten cumulate: the Atok section of the Bushveld Complex. Contrib Miner Petrol 129:20–34

Mayer CC, Jugo PJ, Leybourne MI, Grobler DF, Voinot A (2021) Strontium isotope stratigraphy through the Flatreef PGE-Ni-Cu mineralization at Turfspruit, northern limb of the Bushveld Igneous Complex: evidence of correlation with the Merensky unit of the eastern and western limbs. Miner Deposita 56:59–72

McDonald I, Holwell DA (2007) Did lower zone magma conduits store PGE-rich sulfides that were later supplied to the Platreef? S Afr J Geol 110:611–616

Mitchell AA (2021) Comment on 'Dating the Bushveld Complex: Timing of crystallization, duration of magmatism, and cooling of the World's largest layered intrusion and related rocks' by JS Scoates, CJ Wall, RM Friedman, D Weis, EA Mathez & JA van Tongeren (2021). J Petrol 62(11):1–2. https://doi.org/10.1093/petrology/egaa107

Mitchell AA, Scoon RN (2007) The Merensky Reef at Winnaarshoek, eastern Bushveld Complex: a primary magmatic hypothesis based on a wide reef facies. Econ Geol 102:971–1009

Mungall JE, Kamo SL, McQuade S (2016) U-Pb geochronology documents out-of sequence emplacement of ultramafic layers in the Bushveld Igneous Complex of South Africa. Nature Communication 7:13385

Naldrett A, Wilson A, Kinnaird J, Chunnett G (2009) PGE tenor and metal ratios within and below the Merensky Reef, Bushveld Complex: implications for its genesis. J Petrol 50:625–659

Naldrett A, Kinnaird J, Wilson J, Yudovskaya M and Chunnett G (2011). Genesis of the PGE-enriched Merensky Reef and chromitite seams of the Bushveld Complex. In: Li, C. & Ripley, EM (Eds) Magmatic Ni-Cu and PGE deposits: geology, geochemistry and genesis. Reviews in Economic Geology, 17, 235–296.

Naldrett AJ (1989). Stratiform PGE deposits in layered intrusions. In: Whitney JA and Naldrett AJ (Eds) Ore deposition associated with magmas. Reviews in Economic Geology, 4, 135–166.

Prevec SA, Ashwal LD, Mkaza MS (2005) Mineral disequilibrium in the Merensky Reef, western Bushveld Complex, South Africa: New Sm-Nd isotopic evidence. Contrib Miner Petrol 190:306–325

Roelofse F, Ashwal LD (2012) The lower main zone in the Northern Limb of the Bushveld Complex – a > 1.3 km thick sequence of intruded and variably contaminated crystal mushes. J Petrol 53(7):1449–1476

Roelofse F, Ashwal LD, Romer RL (2015) Multiple, isotopically heterogenous plagioclase populations in the Bushveld Complex suggest mush intrusion. Geochemistry 75(3):357–364

Scoates JS, Wall CJ, Friedman RM, Weis D, Mathez EA, VanTongeren JA (2021) Dating the Bushveld Complex: timing crystallization, duration of magmatism and cooling of the world's largest layered intrusion and related rocks. J Petrol 62:1–39

Scoon RN, Teigler B (1994) Platinum-group elements mineralization in the critical zone of the Western Bushveld Complex: I. Sulphide poor-chromitites below the UG2. Econ Geol 89:1094–1121

Seabrook CL, Cawthorn RG, Kruger FJ (2005) The Merensky Reef, Bushveld Complex: mixing of minerals not mixing of magmas. Econ Geol 100:1191–1206

Smith WD, Maier W, Barnes S, Moorhead G, Reid D, Karykowski B (2021) Element mapping the Merensky Reef of the Bushveld Complex. Geosci Front 12(3):101101

Steiger RH, Jäger E (1977) Subcommission on geochronology: convention on the use of decay constants in Geo- and cosmoschronology. Earth Planet Sci Lett 36:359–362

Trumbull RB, Ashwal LD, Webb SJ, Veksler IV (2015) Drilling through the largest magma chamber on Earth: Bushveld Igneous Complex drilling project (BICDP). Scientific Drilling 19:33–37

Veksler IV, Reid DL, Dulski P, Keiding JK, Schannor M, Hecht L, Trumbull RB (2015) Electrochemical processes in a crystal mush: cyclic units in the upper critical zone of the Bushveld Complex, South Africa. J Petrol 56:1229–1250

Vermaak CF (1976) The Meresnky Reef-thoughts on its environment and genesis. Econ Geol 71:1270–1298

Viljoen M (2016) The Bushveld Complex - host to the world's largest platinum, chromium and vanadium resources. Episodes 39(2):238–268

Willmore CC, Boudreau AE, Kruger FJ (2000) The halogen geochemistry of the Bushveld Complex, Republic of South Africa: implications for chalcophile elements distribution in the lower and critical zones. J Petrol 4:1517–1539

Wilson AH (2012) A chill sequence to the Bushveld Complex: Insight into the first stage of emplacement and implications for the parental magmas. J Petrol 53:1123–1168

Yang SH, Maier WD, Lahaye Y, O'Brien H (2013) Strontium isotope disequilibrium of plagioclase in the upper critical zone of the Bushveld Complex: evidence for mixing of crystal slurries. Contrib Miner Petrol 166:959–974

Yao Z, Mungall JE, Jenkins CM (2021) The Rustenburg layered suite formed as a stack of mush with transient magma chambers. Nat Commun 12:505

Zeh A, Ovtcharova M, Wilson AH, Schaltegger U (2015) The Bushveld Complex was emplaced and cooled in less than one million years – results of zirconology, and geotectonic implications. Earth Planet Sci Lett 418:103–114

Publisher's Note Springer Nature remains neutral with regard to jurisdictional claims in published maps and institutional affiliations.